Study on industrial application of enzymes from extremophiles

(極限環境微生物由来酵素の産業利用に関する研究)

Fina Amreta Laksmi

(2020)

Table of contents

I.

Introduction

The application of enzymes, which is majority obtained from mesophilic organisms, is restricted because of their limited stability to extremes of temperature, pH, and ionic strength [1]. These disadvantages can be addressed by employing the enzymes from extremophiles. Extremophiles are microorganisms that are found in environments of extreme temperature (–2 to 15, 60 to 110 °C), ionic strength (2 to 5 M NaCl) or pH (<4, >9) [1]. Therefore, the use of enzymes isolated from extremophilic microorganisms offers the opportunity to access enzymes that are stable in a variety of different extreme conditions, which can make them more suited to the industrial environments [2]. In this study, a thermophilic L-arabinose isomerase (L-AI) and a halophilic alkaline phosphatase from *Geobacillus stearothermophilus* and *Halomonas* sp. 593, respectively, were used and their properties was improved to cope with industrial application.

L-Arabinose isomerase (L-AI; EC 5.3.1.4) is an enzyme that mainly catalyzes the isomerization reaction between L-arabinose and L-ribulose in L-arabinose catabolism. In addition to L-arabinose isomerization, in 1993, L-AI was also found as a catalyst in the production of D-tagatose, a naturally occurring rare sugar, using D-galactose as a substrate [3]. D-Tagatose has attracted increasing interest as a sucrose substitute and also for many health benefits such as promoting weight loss and growth of intestinal probiotic microbes, reducing the symptoms associated with type 2 diabetes, protecting from tooth decay, and preventing bad breath [4, 5]. Caloric value of D-tagatose is only approximately 38% of the caloric value of sucrose, and it has been shown to not contribute to calorie production [4, 6]. In terms of taste, D-tagatose has a sucrose-like taste with no cooling effect or aftertaste [5]. Further, D-tagatose is 92% as sweet as sucrose, indicating its high similarity to sucrose in terms of sweetness [4]. Furthermore, D-tagatose received generally recognized as safe (GRAS) status from the U.S. Food and Drug Administration in 2001. Therefore, a broad application of D-tagatose in foods, beverages, and pharmaceuticals can be expected [6].

For industrial purpose, biological production of D-tagatose by L-AI requires high thermostability. In an equilibrium process of D-galactose isomerization, elevated temperature is generally favored to shift the reaction toward D-tagatose [7, 8]. Furthermore, higher temperatures should increase reaction rate, improve the substrates solubility, decrease reaction mixture viscosity and reduce microbial contamination [9, 10]. Thermostable L-AIs have been isolated from various thermophilic and hyperthermophilic microorganisms, such as *Thermatoga neapolitana 5068* [11], *Thermatoga maritima* DSM 3109 [12], *Anoxybacillus flavithermus* [13], *Thermoanaerobacter mathranii* DSM 11426 [14], and *Geobacillus thermodenitrificans* [15].

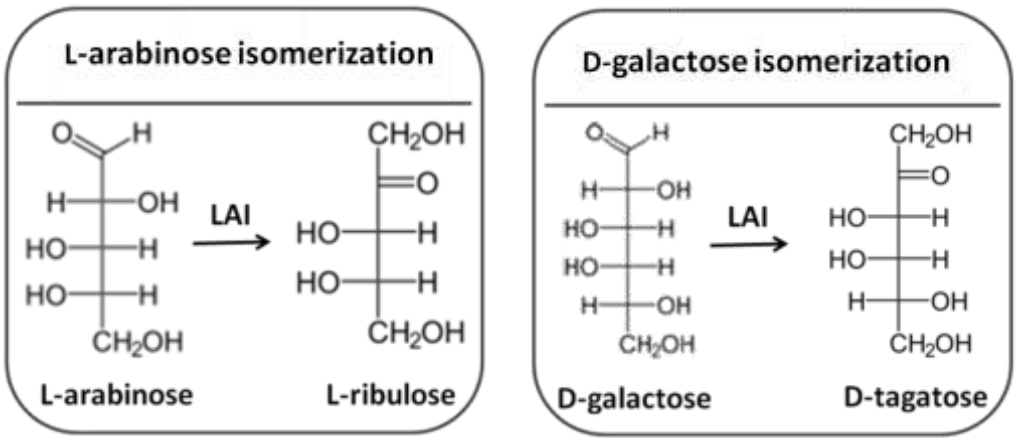

Figure I-1. L-Arabinose isomerase is used as catalyst in the L-arabinose isomerization and D-galactose isomerization.

L-Arabinose is a natural substrate of most L-AIs, and the catalytic efficiency of L-AI for L-arabinose is reported to be approximately 10 times higher than that for D-galactose [16]. In addition to increase the substrate specificity for D-galactose, however, it was suggested that higher stability and activity under slightly acidic condition are desirable, because under alkaline condition, isomerization performed at higher temperatures causes browning

carbonyl-amine reaction known as Maillard reaction and the formation of undesirable by-products [17, 18]. In fact, one of the processes of biological D-tagatose production that has been established requires a slightly acidic condition. With the above process, inexpensive lactose from whey is hydrolyzed into D-galactose and D-glucose by lactase (β-galactosidase) under acidic condition, and then, L-AI converts D-galactose into D-tagatose at elevated temperature [16]. In this approach, a thermostable L-AI that can function in acidic condition is suitable as no pH adjustment is required after hydrolysis reaction. However, most reported thermostable L-AIs were found to be less active at acidic condition than at neutral or alkaline condition [16]. Thus, a thermostable L-AI with the increased substrate specificity toward D-galactose and stable at acidic region (pH 5.0-6.0) is desirable. In order to obtain L-AI that meet with the industrial need, random mutagenesis and site directed mutagenesis will be utilized. In this study, L-AI isolated from a thermophilic microorganism, *Geobacillus stearothermophilus* (GSAI), was used.

Halophilic enzymes are useful for industrial applications for the following reasons. (1) They are more efficient at increasing the salt concentration, which can prevent the survival and growth of non-halophilic bacteria causing food poisoning and putrefaction. (2) At high salt concentrations, halophilic enzymes may not have to be purified or sterilized as part of their preparation, as contaminating proteins or other biological molecules are not functional. (3) Many of these enzymes can work, as expected, under conditions of low water activity and can function in organic solvents, although the reason for this has yet to be clarified. (4) Some of them also function at elevated temperatures [19–22]. However, these enzymes are easily degraded when used for industrial applications compared with thermophilic and alkaliphilic enzymes because of their instability in low-salt environments. Given this instability in a low-salt environment, the expression in non-halophilic hosts and purification are also difficult, which has inhibited the progression of the study of halophilic enzymes. In this study, we

aimed to secrete the halophilic enzyme alkaline phosphatase (ALPase) isolated from *Halomonas* sp. 593 (HaALP) [23, 24] from Gram-positive non-halophilic *Brevibacillus choshinensis* and to study its stabilization and folding mechanisms.

II.

Improved substrate specificity for D-galactose of L-arabinose isomerase

II-1. Introduction

L-Arabinose is a natural substrate of most L-AIs, and the catalytic efficiency of L-AI for L-arabinose is reportedly around 10 times higher than that for D-galactose [16]. Thus, modification of L-AI to improve its substrate specificity for D-galactose is desirable. D-galactose is bigger in size with six carbon atoms than L-arabinose with five carbon atoms. Based on this condition, we intend to create a widen space or enhance the flexibility around the binding pocket of GSAI. Hopefully, it could increase the substrate specificity of GSAI toward D-galactose since the bigger size of D-galactose might be better fitted on the GSAI binding pocket.

To create a widen space or enhance the flexibility around the binding pocket of GSAI, Molecular Operating Environment software (MOE) will be utilized. Moreover, the crystal structure of the thermophilic L-AI, *Geobacillus kaustophilus* arabinose isomerase (GKAI) [25], has been reported and provides a better understanding of the relationship between L-AI structure and function. Hence, the crystal structure of L-arabitol bound GKAI will be used as the template based on the high similarity (99%) and high identity (97%) between the GKAI and the GSAI. By observing amino acids around binding pocket (more specifically amino acids near C3-C5 and O3-O5 of L-arabitol) while avoiding the amino acids near the active site (around C1 and C2) and the important amino acids for binding, we decided to generate mutants by altering amino acid residues at 4 different sites (H18, N123, Q126 and M350). The initial amino acid residues at those sites will be altered to the smaller amino acid residues. Characterization of promising mutant was investigated by determining its kinetic parameters compared with wild-type (WT). The structure models of the promising mutant and WT were constructed to provide insight into the effect of the mutation on the binding pocket. The addition of borate during D-galactose isomerization was also evaluated.

II-2. Materials and methods

II-2.1. Strains, plasmids, and medium

Escherichia coli JM109 and *E. coli* BL21 Star (DE3) were used for cloning and protein expression, respectively. They were cultured in Lysogeny Broth medium (LB)–ampicillin (100 $\mu g mL^{-1}$). The plasmid pET15b–GSAI, constructed by inserting WT L-arabinose isomerase from *Geobacillus stearothermophilus* into pET15b (Novagen), was used as the expression vector. Transformants harboring an expression vector were precultured in LB–ampicillin containing 0.4% glucose.

II-2.2. Selection of potential amino acid residues in the binding pocket area

The following procedure for the selection of potential amino acid residues in the binding pocket was carried out using MOE software (Chemical Computing Group). The crystal structure of L-arabitol-bound GKAI was used as the template (PDB ID: 4R1Q) [16] to observe the amino acid residues of GSAI in the binding pocket area. The GKAI crystal structure was chosen on the basis of the high similarity (99%) and high identity (97%) between GKAI and GSAI. All the residues near C3, C4, C5, O3, O4, and O5 of L-arabitol were examined by alanine scanning in an Amber10:Extended Huckel Theory (EHT) force field in MOE to calculate the substrate affinity of each residue. Only residues that had little or no effect on affinity and therefore could not bind to the substrate were selected as potential candidates for mutation. The stability of the single-site variants was investigated using residue scanning in an Amber10:EHT force field. Variants that did not destabilize were used for site-directed mutagenesis.

II-2.3. Expression and purification of L-AI

The araA gene encoding L-AI was amplified by polymerase chain reaction (PCR) using pGEM-T Easy-GSAI [26] as a template. The amplified fragment was cloned into NdeI/BamHI-digested pET15b. The araA gene contains an NdeI site at position 1045. Hence, partial digestion of the amplified fragment was conducted to prevent cutting at an unfavorable position. The constructed plasmid, pET15b–GSAI, containing the araA gene was sequenced using an ABI PRISM 3500xL Genetic Analyzer (Applied Biosystems). *E. coli* BL21 Star (DE3) harboring pET15b–GSAI was precultured in LB–ampicillin containing 0.4% glucose at 37 °C, with shaking at 160 rpm overnight. The 1% preculture was added to 100 mL LB–ampicillin, and the culture was incubated at 18 °C with shaking at 130 rpm. After the culture reached an optical density of 1.0 at 600 nm, 0.2 mM isopropyl-β-D-thiogalactopyranoside (IPTG) was added to induce the synthesis of GSAI. After an overnight incubation at 18 °C with shaking at 130 rpm, the cells were collected by centrifugation and resuspended in 50 mM Tris-HCl buffer (pH 8.0). The cells were disrupted by sonication, and the obtained supernatant was applied to a HisTrap™ HP (1 mL; GE Healthcare) column. The bound protein was eluted with a linear gradient of 20–500 mM imidazole in a 20 mM sodium phosphate buffer (pH 7.4) at a flow rate of 1 mL min^{-1}. After the purification by Ni-affinity chromatography, fractions containing targeted enzyme were further purified by ion exchange chromatography using a HiTrap™ Q HP (1 mL; GE Healthcare) column. An Äkta prime system (GE Healthcare) was used to carry out the chromatographic purification. The desired fractions were dialyzed against 50 mM Tris-HCl buffer (pH 7.5) to remove imidazole. The purity of GSAI was confirmed by sodium dodecyl sulfate polyacrylamide gel electrophoresis (SDS-PAGE) on a 10% gel according to the method of Laemmli [27]. The protein

concentration was examined using the bicinchoninic acid (BCA) method, with bovine serum albumin as the protein standard [28].

II-2.4. Site-directed mutagenesis

Site-directed mutagenesis was performed in accordance with the QuikChange® II XL Site-Directed Mutagenesis Kit (Stratagene) protocol, with several modifications. The mutant strands were synthesized by PCR using 125 ng of two complementary mutagenic primers (Table 1) and 10 ng pET15b–GSAI as a template. The mutagenic primers were designed to generate several amino acids, replacing the original residue at the point of mutation (Table II-1). The following PCR cycle was used to generate mutants: 98 °C for 1 min, followed by 18 cycles of 98 °C for 50 s, 60 °C for 50 s, 68 °C for 4 min, and 1 cycle of 68 °C for 4 min for the final step. The amplified mutant strand was treated with *Dpn*I at 37 °C for 2 h to digest the methylated parental template. The *Dpn*I-digested PCR product was transformed into *E. coli* BL21 Star (DE3) and cultured overnight at 37 °C on LB–ampicillin plates containing 0.4% glucose.

Table II-1. Primer used in the site-directed mutagenesis. The restriction site and the site of mutation in the sequence alignment of the primers were marked by underline. Bold letters shows the potential candidate amino acids selected using the residue scanning.

Primer (forward, 5' to 3')	Usage
GTAACGGGAAGCCAGRBCTTGTACGGAGAAGAAG	Mutagenesis for GSAI H18**A**/**T**/**S**/**V**/N/I/D/G
CGATATGGACTTTATGRBCTTAAACCAATCGGC	Mutagenesis for GSAI N123**A**/**T**/**S**/**V**/I/G
CTTTATGAACTTAAACDYATCGGCTCACGGTGAC	Mutagenesis for GSAI Q126**A**/**T**/**S**/**V**/I/L
CTCGGCGCTCATDYGCTCGAAGTATGTC	Mutagenesis for GSAI M350**A**/**T**/**S**/**V**/M/L

II-2.5. Screening

Colonies harboring pET15b containing the mutated GSAI gene obtained from the transformation were screened in a 96-well plate. These colonies were transferred to a 96-well plate containing 200 μL LB–ampicillin medium and cultured at 18 °C overnight with shaking at 10000 rpm overnight (Mix-EVR, TAITEC). To induce the synthesis of L-AI, 0.2 mM IPTG was added and cells were harvested by centrifugation after a 10 h incubation at 18 °C with shaking at 10000 rpm. The cells were resuspended in 21.1 μL of 50 mM Tris-HCl buffer (pH 8.0) and frozen at −80 °C for 1 h. L-AI was extracted by thawing at 60 °C for 30 min. Subsequently, the activity was measured as follows: a mixture of 26.4 μL containing 3 μL of sample, 50 mM D-galactose, 1 mM $MnCl_2$, and 50 mM Tris-HCl buffer (pH 8.0) was incubated at 60 °C for 30 min, and the amount of D-tagatose was determined after treatment with cysteine–carbazole–sulfuric acid [29] using a Benchmark Plus™ Microplate Spectrophotometer (Bio-Rad Laboratories) at 560 nm.

II-2.6. Enzyme activity assay

A standard assay for determining the activity of L-AI was carried out with 50 mM L-arabinose and 1 mM $MnCl_2$ in 50 mM Tris-HCl buffer (pH 8.0) at 60 °C for 30 min and immediately stopped with the addition of the sulfuric acid contained in the cysteine–carbazole–sulfuric acid solution. In addition to stopping the reaction, it was also used for coloring the reaction, enabling the quantification of L-ribulose and D-tagatose at an absorbance of 560 nm [29]. The standard curves for D-tagatose and L-ribulose were plotted in 50 mM Tris-HCl buffer (pH 8.0) or 200 mM borate buffer (pH 8.0), from 0 to 0.05 μmol and

from 0 to 0.5 μmol, respectively. The substrate specificity of WT enzyme and mutants for L-arabinose and D-galactose was determined in 50 mM Tris-HCl buffer (pH 8.0) or 200 mM borate buffer (pH 8.0), respectively, containing 50 mM substrate and 1 mM $MnCl_2$. The amount of enzyme used was 1 and 5 μg for the determination of specificity for L-arabinose and D-galactose, respectively. The reaction was incubated at 60 °C for 30 min.

II-2.7. Determination of thermal property

To determine the optimum temperature for the activity of WT and mutant enzymes, the temperature was varied from 30 °C to 80 °C. The enzymatic activity assay for examining the optimum temperature was performed as described above. For investigation of the thermostability of the enzyme, the enzyme (0.01 μg μL^{-1}) was incubated at 30–80 °C for 1 h. The incubation was stopped by cooling on ice, and the residual activity was measured as described above.

II-2.8. Determination of kinetic parameters

To determine the kinetic parameters of the WT enzyme and mutants, 10–200 mM D-galactose and 5–100 mM L-arabinose were used. A mixture of 50 mM Tris-HCl buffer (pH 8.0) containing substrate, and 1 mM $MnCl_2$ was incubated with enzyme at 60 °C for 30 min. To investigate the kinetic parameters in borate, 50mM Tris-HCl buffer (pH 8.0) was replaced with 200mM borate buffer (pH 8.0). The amount of enzyme added was 1 and 5 μg when L-arabinose and D-galactose, respectively, were used in the reaction. The kinetic parameters of the enzymes (K_m (mM), k_{cat} (min^{-1}), and V_{max} (U mg^{-1})) for L-arabinose and D-galactose were

determined with Michaelis–Menten plots (V vs [S]) using GraphPad Prism 7 (GraphPad software).

II-2.9. Modeling and validation of H18T

Modeling of WT GSAI and mutant GSAI (H18T) was performed using the Coot program [30], with the 3D structure of GKAI from *Geobacillus kaustophilus* (PDB ID: 4R1Q) [25], which has high similarity (99%) and high identity (97%) with GSAI, as the template. Because the structure of GSAI has 12 different amino acid residues to GKAI (K26, R33, I34, M35, W39, F49, V78I, N208, R361, V364, S481, and K488), 4R1Q was converted to the GSAI model by introducing these 12 residues (R26, M33, M34, I35, L39, L49, I78, S208, K361, I364, P481, and R488), and the H18T model, which involved one point mutation (H18T), was subsequently constructed from the GSAI model. In both the GSAI and H18T modeling, amino acid mutations were placed so that the dihedral angles of the side chain were conserved. The structural fitness of the side chain of the mutated residues was inspected using rotamer analysis by the Coot program. The rotamer probabilities of the mutated residues in the GSAI and H18T models were above 98.3% (Table II-2).

Ramachandran analysis using the Rampage program [31] was also used to validate the conformations of the GSAI and H18T models. The results of Ramachandran analysis for the GSAI and H18T models are shown in Fig. II-1 and Table II-3. Both the GSAI and H18T models have 97.4% of the residues in the favored conformation in a Ramachandran plot and no residues in the outlier region (Table II-3). The K26R, R33M, I34M, M35I, W39 L, F49 L, V78I, N208S, R361K, V364I, S481P, K488R, and H18T mutations did not change the favorability (Table II-3). Finally, the hexamer model was constructed by superimposing chain

A on chains B, C, D, E, and F of 4R1Q origin using secondary-structure matching of the Coot program.

Table II-2. Rotamer probability of mutagenized residues in the WT GSAI model and mutant GSAI (H18T) model prepared in this study.

	No. of mutation site	Residue	Rotamer probability (%)
WT GSAI	26	R	99.9
	33	M	100
	34	M	100
	35	I	98.3
	39	L	100
	49	L	100
	78	I	98.3
	208	S	100
	361	K	100
	364	I	98.3
	481	P	99.0
	488	R	99.9
H18T	18	T	96.7

Table II-3. Structure model validation of 4R1Q (GKAI), WT GSAI, and H18T based on Ramachandran plot.

	4R1Q	WT GSAI (K26R, R33M, I34M, M35I, W39L, F49L, V78I, N208S, R361K, V364I, S481P, K488R)	H18T
Number of residues in favored region (~98.0% expected)	480 (97.4%)	480 (97.4%)	480 (97.4%)
Number of residues in allowed region (~2.0% expected)	13 (2.6%)	13 (2.6%)	13 (2.6%)
Number of residues in outlier region	0 (0.0%)	0 (0.0%)	0 (0.0%)

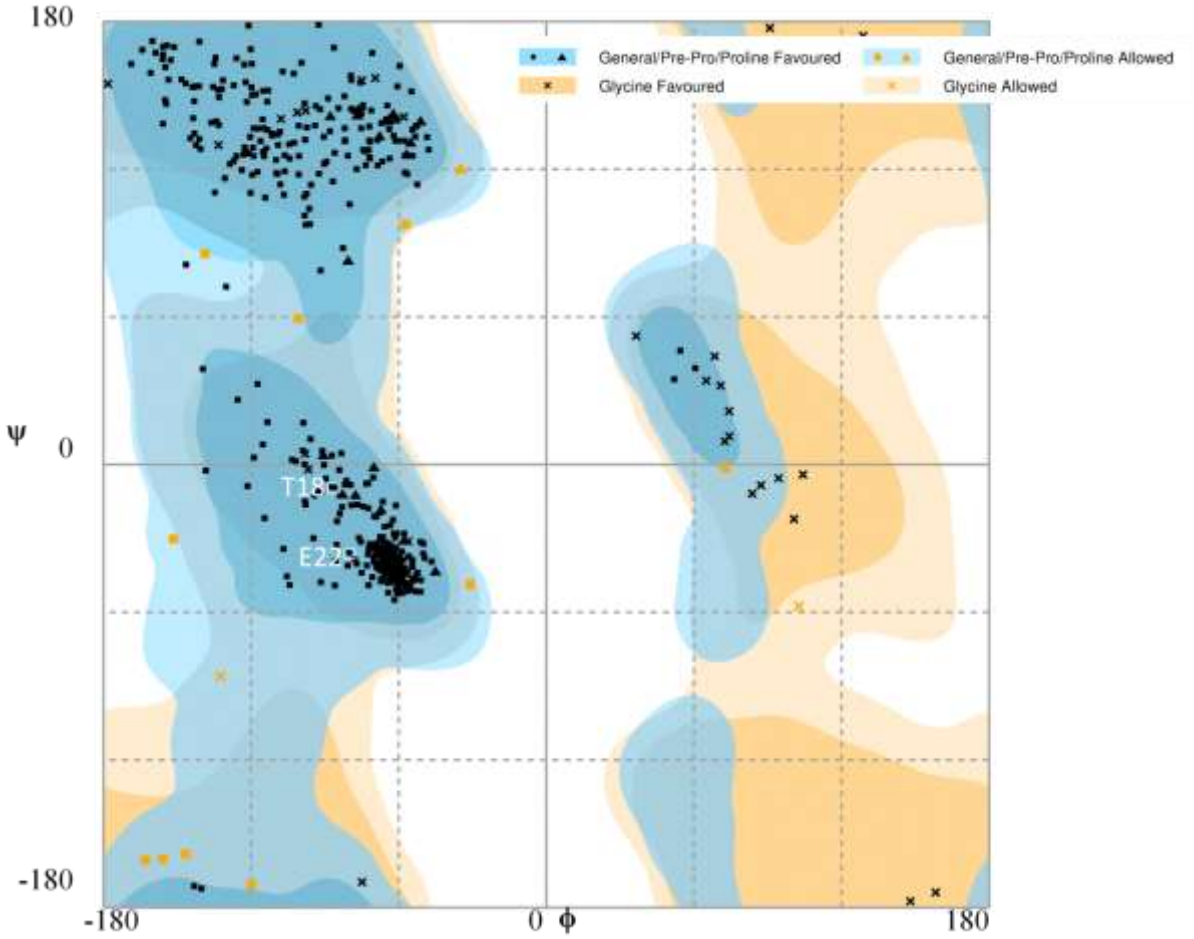

Figure II-1. Steric validation of the WT and H18T models by the Ramachandran plot. White letters represent the mutated residue (T18) and the original residue (E22) involved in the formation of hydrogen bonds with residue 18.

The volumes of binding pockets around the active site and mutation site were calculated using the program POCASA [32]. The elastic network model-based normal mode analysis (NMA) using the program PDBη [33] was also conducted to derive protein dynamics information, especially the time average of the dihedral angle fluctuation, from GSAI and H18T models. All normal modes of GSAI (2350 modes) and H18T (2349 modes) were calculated, and perturbations were applied to evaluate the time average of the dihedral angle fluctuation.

II-3. Results

II-3.1. Selection of candidate residues for mutation

To increase the substrate specificity of GSAI for D-galactose, it is probably necessary to create a wider space at the binding pocket of GSAI and to improve the flexibility around the binding pocket as D-galactose is larger than L-arabinose, with six carbon atoms instead of five. To address this, amino acids that may have little or no effect on the affinity of GSAI were replaced with smaller amino acids because mutations that modify the substrate binding pockets often place a larger stability burden than surface mutations, and the evolution of new enzymatic specificities is accompanied by the loss of the protein's thermodynamic stability as reported by Tokuriki et al. [34]. Therefore, in our first attempt, in addition to obtain a variant with improved substrate specificity for D-galactose, we tried to change the amino acid into one that prevents the variant from destabilization. Examination of amino acid residues around the binding pocket was first conducted using the crystal structure of L-arabitol-bound GKAI (PDB ID: 4R1Q) [25]. Fourteen residues around C3, C4, C5, O3, O4, and O5 of L-arabitol, which were identified as Q17, H18, L19, Y20, F84, N123, Q126, H129, M186, E307, E332, Y334, M350, and I371, were chosen as the candidate residues for alanine scanning using MOE software (Fig. II-2). Residues near C1, C2, O1, and O2 that may be important for the substrate binding of GSAI were excluded from the examination. Next, on the basis of alanine scanning of the chosen residues, residues that had a delta affinity value from 0 to 2 kcal mol^{-1} were selected, as they may have little or no effect on the substrate binding of GSAI, which would avoid decreased activity of GSAI after mutation (Fig. II-3). Four residues, H18, N123, Q126, and M350, qualified and were chosen for the next assessment: residue scanning. Residue scanning was performed to investigate the structural stability if the original amino

acid residue was replaced with other amino acids. Residue scanning using MOE software showed that changing the original amino acid at selected sites into alanine, valine, threonine, or serine could maintain the stability of the enzyme. Moreover, these four amino acids are smaller in size than histidine, glutamine, asparagine, and methionine, indicating that they were suitable candidates for mutation.

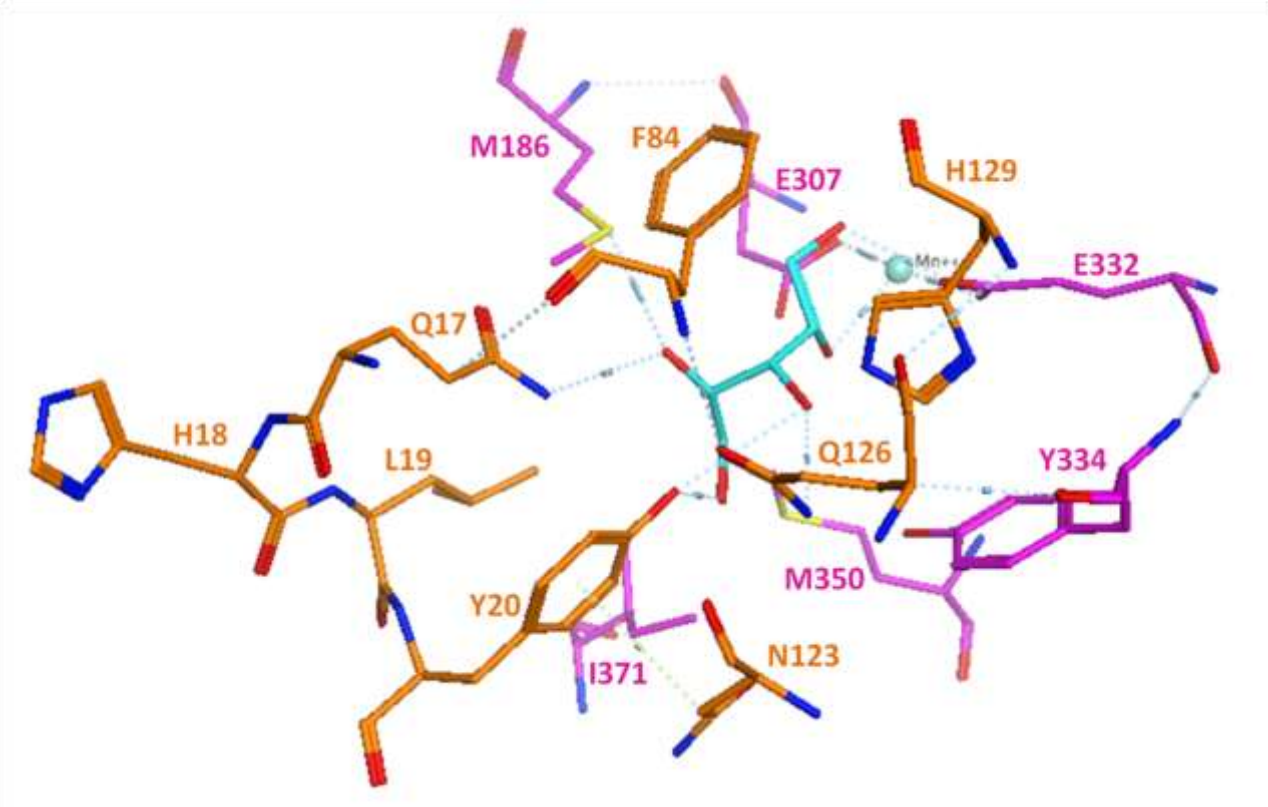

Figure II-2. Amino acid residues around the binding pocket of *Geobacillus kaustophilus* L-AI (GKAI) complexed with L-arabitol. The crystal structure of L-arabitol-bound *Geobacillus kaustophilus* L-AI (GKAI) (PDB ID: 4R1Q) [17] was used as the template. The orange and pink sticks represent subunits of GKAI. Amino acid side chains are colored by atom type (oxygen in red, nitrogen in blue, and sulfur in yellow). Mn^{2+}, H-bond and H-pi bond are shown as a light blue sphere, dotted lines in light blue, and dotted line in light green, respectively. The substrate, L-arabitol, is depicted as a light blue stick.

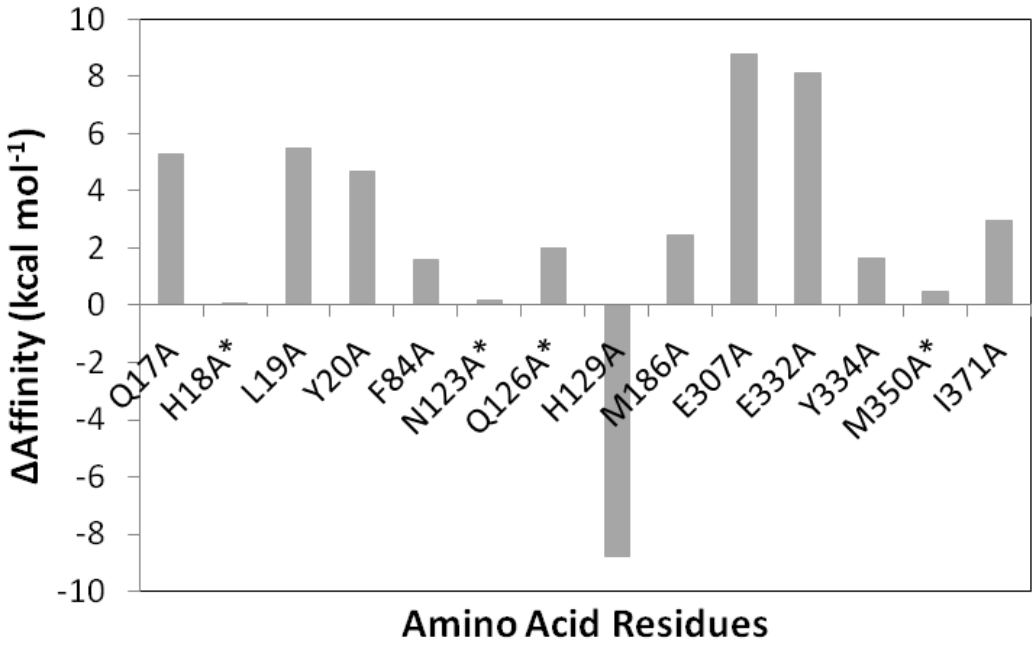

Figure II-3. Alanine scanning of amino acid residues at the binding pocket of *Geobacillus stearothermophilus* L-AI. The effects of single mutations on the Δaffinity of 14 residues were calculated using MOE software. Asterisk indicates the selected residues for mutation.

II-3.2. Selection of potential variants with improved substrate specificity for D-galactose

Mutation into alanine, threonine, serine, and valine was performed at each selected residue and identified as H18A/T/S/V, N123A/T/S/V, Q126A/T/S/V, and M350A/T/S/V. Further, on the basis of the construction of the mutagenic primer (Table II-1), mutation into other amino acids could also be performed, e.g., H18N/I/D/G, N123I/G, Q126I/L, and M350 M/L, resulting in a total of eight mutant variants for residue at position 18, which were identified as H18A/T/S/V/N/I/D/G, and six mutant variants for residue at positions 123, 126, and 350, which were identified as N123A/T/S/V/I/G, Q126A/T/S/V/I/L, and M350A/T/S/V/M/L, respectively, obtained from site-directed mutagenesis using mutagenic primers. Colonies

harboring variant L-AI genes collected after transformation were screened in a 96-well plate. Only two strains with mutations at position 18 that exhibited higher activity for D-galactose than WT could be obtained from the screening. However, assessment of activity for D-galactose at positions 123 and 350 showed decreased activity by almost all the investigated strains. In the case of mutation at position 350, strains that displayed activity similar to the control were shown to be WT after DNA sequencing, and it was likely the same with N123. When mutation at amino acid 126 was performed, a significantly lower activity was observed for all the investigated strains. On the basis of these results, mutations at position 123, 126, and 350 of GSAI may cause structural instability or unfavorable turnover of substrate. Thus, a total of two strains harboring a mutation at residue 18 that demonstrated improved activity for D-galactose were acquired, on the basis of screening in a 96-well plate. To confirm this result, the two potential strains were grown in 5 mL of LB–ampicillin medium, and the activity of the extracted enzymes was measured. The newly expressed variants of mutated L-AI at residue 18 confirmed the first screening result in the 96-well plate; the substrate specificity for D-galactose of these variants was 1.3–1.5-fold higher than that of WT. The mutated L-AI genes were extracted from the two potential strains, and DNA sequencing was conducted to identify the mutations. DNA sequencing of the two strains showed that the histidine at position 18 was changed to threonine and serine, and they were designated as H18T and H18S, respectively.

3.3. Assessment of the structural stability of potential variants

The H18T and H18S variant enzymes demonstrated higher activity for D-galactose than WT. Nevertheless, introducing mutations often causes the loss of structural stability in exchange for desirable quality. Therefore, further investigation of their biochemical

properties was performed to observe the effects of the mutation on their stability. Pure L-AIs were required to perform the assay, so recombinant L-AIs with an N-terminal His-Tag attached during their construction were purified by Ni-affinity chromatography. The purified fractions were used to determine the activity for D-galactose and L-arabinose. Both variants showed increased relative activity for D-galactose of up to approximately 40% compared with WT. This result confirmed the previous screening result that they exhibited improved substrate specificity for D-galactose.

The temperature dependence and stability of the variant L-AIs were determined (Fig. II-4). The temperature dependence was measured in 50 mM Tris-HCl buffer (pH 8.0) containing 50 mM L-arabinose and 1 mM $MnCl_2$ at 30 °C–80 °C for 30 min, whereas the thermostability of the enzyme was quantified as the residual activity after 1 h incubation at 30 °C–80 °C. As shown in Fig. II-4A, at 60 °C, H18T and WT showed the highest activities of 3.85 and 3.88 U mg^{-1}, respectively. H18S achieved its maximum activity, 3.44 U mg^{-1}, at 50 °C, which was lower compared with the maximum activity of H18T and WT. The activity of H18T slightly shifted at a higher temperature, and it could maintain activity (2.63 U mg^{-1}) at 70 °C compared with WT (1.54 U mg^{-1}) and H18S (1.69 U mg^{-1}). This indicated that the mutation from histidine to threonine at position 18 resulted in slightly better performance at higher temperatures. The thermal stability of H18T and H18S compared with WT is shown in Fig. II-4B. The stability of H18T and H18S remained high (> 80%) at 60 °C, but at temperatures higher than 60 °C their structure was significantly degraded. A similar denaturation profile was displayed by WT enzyme, suggesting that mutation at position 18 of GSAI hardly affected its overall structural stability. Regardless of the lack of destabilization for both H18T and H18S, H18T was more favorable for D-tagatose production at higher temperatures. Previous reports suggested that a thermostable L-AI was required to overcome

the energy barrier for D-galactose isomerization [7, 8], which was shown by H18T. Thus, H18T was chosen for further investigation of its kinetic properties.

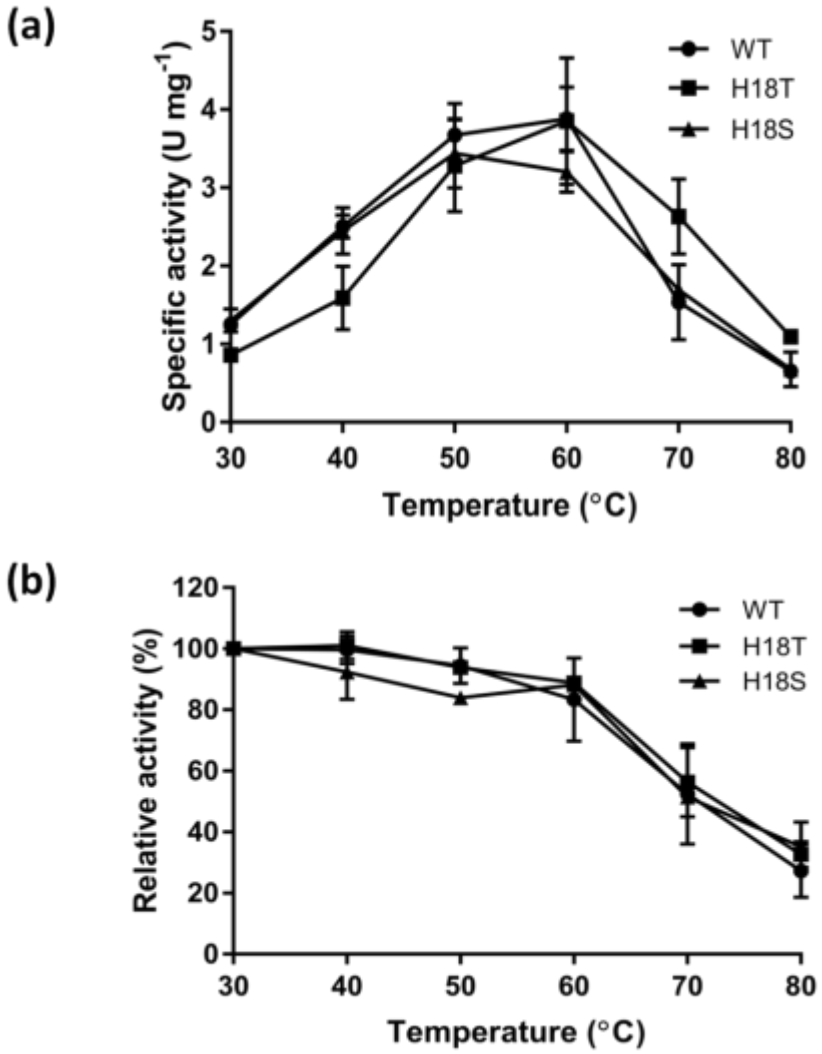

Figure II-4. Thermal stability of the variant L-AIs at position 18 of *Geobacillus stearothermophilus* for L-arabinose isomerization. (a) Optimum reaction temperature of variant L-AIs was determined at 30–80°C. (b) The residual activity was measured after incubation at 30–80°C for 1 h. Values represent the mean of triplicate experiments ± standard deviation.

II-3.4. Purification and characterization

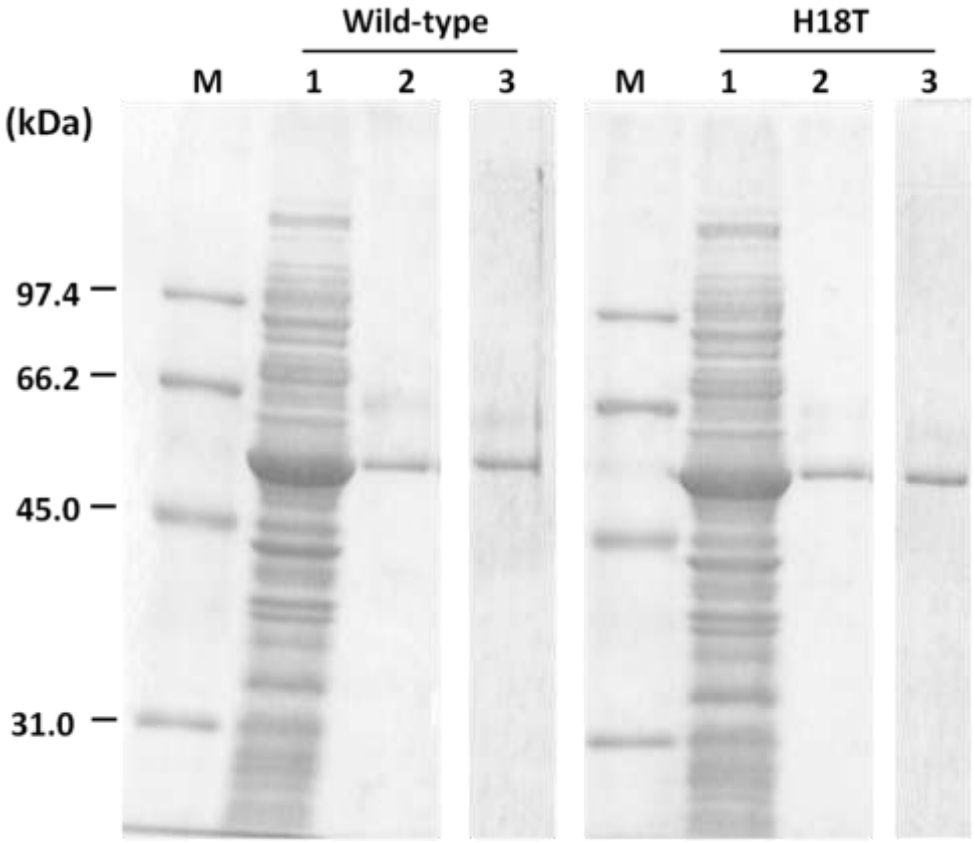

Figure II-5. SDS-PAGE analysis of wild-type GSAI and variant L-AIs expressed in *E. coli* BL21 Star (DE3) using 10% acrylamid gels. Lanes: M, molecular weights; 1, crude cell-free extracts; 2, purified fraction after HisTrap™ HP chromatography; 3, purified fraction after HiTrap™ Q chromatography.

H18T was selected as the potential candidate with improved substrate specificity for D-galactose. Its characteristics were determined by measuring its kinetic parameters compared with WT. Before characterization, a two-step purification was performed to obtain quite a high purity of the enzymes. H18T and WT were first expressed in *E. coli* BL21 star (DE3) in a scale-up medium, 100 mL of LB–ampicillin, and their crude extracts were purified

by Ni-affinity chromatography (HisTrap™ HP) and then ion exchange chromatography (HiTrap™ Q HP). SDS-PAGE was used to analyze the proteins obtained at each purification step. The purity of the L-AI variants was successfully obtained, and the molecular mass of the L-AI variants was estimated to be approximately 58 kDa by SDS-PAGE (Fig. II-5), in accordance with the molecular weight predicted from the amino acid sequence. There are 17 additional residues in the N-terminus derived from the His-Tag fragment: the thrombin site, residues between the His-Tag and the thrombin site, and the NdeI site, which caused the molecular weight of the N-terminal His-Tag fusion L-AI variants to be approximately 2 kDa larger than L-AI without the His-Tag (approximately 56 kDa).

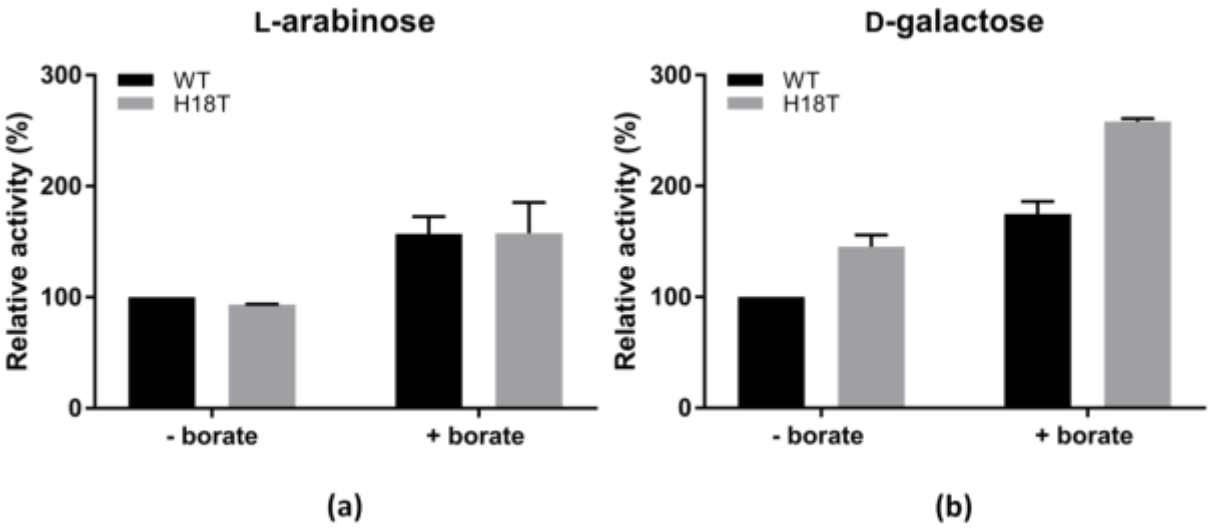

Figure II-6. Activities of the variant L-AIs at position 18 of *Geobacillus stearothermophilus*. (a) L-Arabinose and (b) D-galactose isomerization. Values represent the mean of triplicate experiments ± standard deviation.

Investigation of the substrate specificity of H18T for L-arabinose indicated a decrease in its relative activity of about 7%. This negligible decrease in the activity of H18T indicated that mutation at residue 18 from histidine to threonine hardly affected the activity when L-

arabinose was used as the substrate (Fig. II-6A). Addition of borate during L-AI catalysis is known to normally facilitate higher conversion toward ketoses, as it forms complexes better with ketoses than with aldoses [35, 36, 37]. As shown in Fig. II-6A, WT exhibited 57.15% higher relative activity for L-arabinose with the addition of borate. Similarly, H18T attained 64.7% higher relative activity.

When D-galactose was used as the substrate, the substrate specificity of WT and H18T was 100% and 145.4%, respectively (Fig. II-6B). This demonstrated that the mutation from histidine to threonine at position 18 improved the substrate specificity for D-galactose by up to 45.4%. The relative activity of H18T and WT further increased in the presence of borate. WT achieved 74.9% higher relative activity for D-galactose, whereas H18T attained 112.7% higher relative activity. Overall, when borate was added during the isomerization of D-galactose to D-tagatose, the relative activity of H18T for D-galactose improved by up to 158.1% compared with WT without borate.

A role for the mutation in improved substrate specificity for D-galactose was hypothesized on the basis of the comparison of kinetic parameters between WT and H18T. To determine the kinetic parameters of H18T compared with WT for both L-arabinose and D-galactose, Michaelis–Menten plots were used (Fig. II-7). All the results derived are summarized in Table 1. Investigation of the kinetic parameters of H18T for L-arabinose indicated that both K_m and k_{cat} of H18T were slightly higher than those of WT. As a result, the catalytic efficiency (k_{cat}/K_m) and the specific activity of H18T were similar to those of WT, suggesting that mutation at residue 18 likely caused negligible effects when L-arabinose was used as the substrate. In contrast, K_m and k_{cat} of H18T for D-galactose were 0.4-fold and 0.7-fold lower, respectively, than those of WT. The decrease of both K_m and k_{cat} resulted in an increased catalytic efficiency and specific activity of H18T of up to 1.8-fold and 1.5-fold,

respectively, indicating that the D-galactose binding affinity of H18T at the binding pocket was improved.

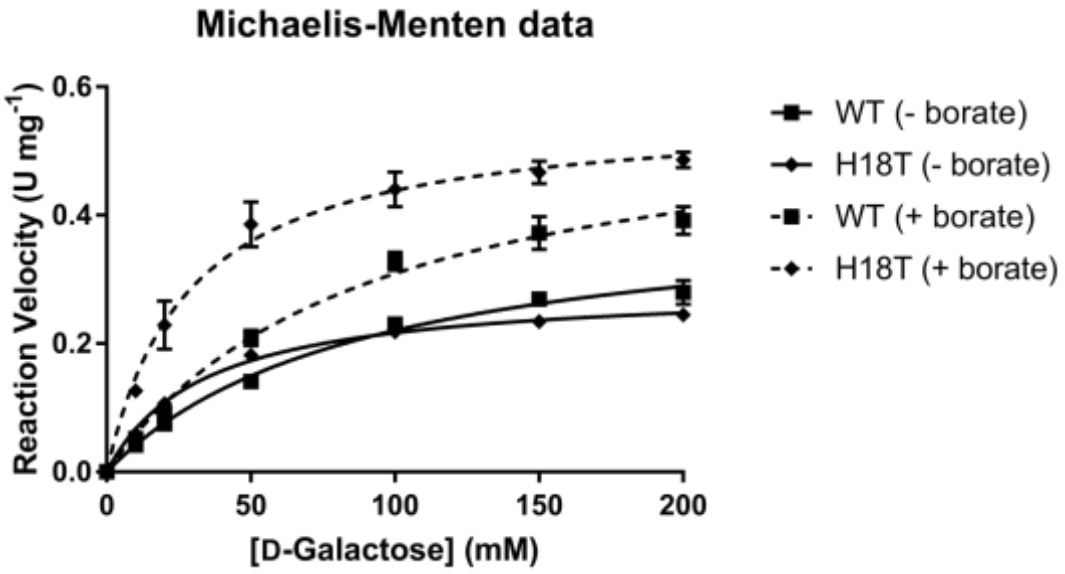

Figure II-7. Michaelis–Menten kinetics of variant L-AIs in the presence and absence of 200 mM borate buffer. The kinetic parameters were determined by incubating in 50 mM Tris-HCl buffer or 200 mM borate buffer containing 0, 10, 20, 50, 100, 150, and 200 mM D-galactose and 1 mM $MnCl_2$ at 60°C for 30 min. Values represent the mean of triplicate experiments ± standard deviation.

Investigation of the effect of the addition of borate on D-tagatose conversion is also shown in Table II-4. In the presence of borate, WT demonstrated a similar K_m as without borate. In contrast, the k_{cat} of WT showed a 1.4-fold increase after the addition of borate, resulting in an increased catalytic efficiency and specific activity of about 1.5-fold, respectively. In the case of H18T, it also possessed a similar K_m as without borate, but the k_{cat} showed a 2.0-fold increase. This caused the catalytic efficiency and specific activity to

increase by around 2.0-fold, respectively. In summary, the effect of enhancing D-tagatose production by the addition of borate was higher for the H18T mutant than for the WT enzyme.

Table II-4. Kinetic Parameters of H18T variant of *Geobacillus stearothermophilus*.

	WT					H18T				
Substrate	**Specific activity (U mg^{-1})**	**K_m (mM)**	**k_{cat} (min^{-1})**	**V_{max} (U mg^{-1})**	**k_{cat}/K_m (mM^{-1} min^{-1})**	**Specific activity (U mg^{-1})**	**K_m (mM)**	**k_{cat} (min^{-1})**	**V_{max} (U mg^{-1})**	**k_{cat}/K_m (mM^{-1} min^{-1})**
L-arabinose	4.51	8.60	282	5.00	32.9	4.21	12.8	367	6.50	28.6
D-galactose	0.14	90.6	23.6	0.42	0.26	0.20	33.5	16.2	0.29	0.48
With borate										
D-galactose	0.24	90.7	33.1	0.59	0.36	0.37	28.4	31.6	0.56	1.11

(n=3)

II-4. Discussion

D-Tagatose production via an enzymatic pathway instead of a chemical process has gained interest recently, as it is a friendlier environmental process with fewer undesirable byproducts [35]. In the enzymatic production of D-tagatose, L-AI (EC 5.3.1.4) is used as the catalyst, with D-galactose as the substrate [3]. Hence, we investigated the substrate specificity of L-AI from *Geobacillus stearothermophilus* (GSAI) for L-arabinose and D-galactose. The result of our investigation showed that the substrate specificity for L-arabinose was around 6-fold higher than that for D-galactose, which is in accordance with a previous report where L-arabinose is the natural substrate of most L-AIs [16]. However, this condition is unfavorable for industrial applications. Thus, improvement of the substrate specificity of L-AI was required to enhance the production of D-tagatose. *In silico* studies on the substrate specificity of an L-arabinose isomerase from *Bacillus licheniformis* showed that the unfavorable k_{cat} value for D-galactose is likely related to the size of binding pocket area. A deeper and wider binding pocket may accommodate a large size of D-galactose that results in a better turnover value for D-galactose compared with the narrow binding pocket [38]. On the basis of this, to increase the substrate specificity for D-galactose, a larger or more flexible binding pocket was desirable as D-galactose is larger than L-arabinose, with six carbon atoms instead of five. The introduction of mutations around the binding pocket of GSAI was performed to achieve this.

The analysis of residues around the binding pocket of GSAI was performed using MOE software to select mutation sites. The mutations were introduced using saturation mutagenesis, and mutants that showed high activity for D-galactose were screened. A mutant, H18T, was chosen as the successful candidate for the production of D-tagatose. The mutation at residue 18 caused a 0.4-fold lower K_m of H18T compared with WT. The higher binding affinity of H18T led to an increased specific activity and catalytic efficiency. Furthermore,

H18T facilitated higher D-tagatose conversion in the presence of borate. When borate was added to the reaction mixture, H18T exhibited higher specific activity and catalytic efficiency of about 1.8-fold and 2.3-fold, respectively, compared with H18T in the absence of borate. In case of the WT, the addition of borate caused an improvement of specific activity and catalytic efficiency of about 1.8-fold and 1.4-fold, respectively, compared with WT in the absence of borate. Overall, we successfully obtained a mutant (H18T) that possessed 1.5-fold and 3.1-fold higher specific activity and catalytic efficiency, respectively, in the presence of borate compared with WT in the presence of borate. In addition, H18T maintained its thermal stability, which is beneficial for D-tagatose production as it requires a high temperature (60 °C–70 °C) to shift the equilibrium toward D-tagatose.

A previous report on the modification of L-AI from *Geobacillus thermodenitrificans* demonstrated a remarkable improvement of substrate specificity for D-galactose [39]. The catalytic efficiency of the triple-site variant, identified as F280 N, for D-galactose was 9.4-fold higher than that of WT, whereas H18T displayed an approximately 2-fold higher catalytic efficiency than WT, which was lower than that of F280 N. In terms of the kinetic parameters, F280 N showed an increase of k_{cat} value by 30-fold for D-galactose. Investigation of the position of the mutated residue revealed that residue 280 was located on the binding pocket area and N280 directly interacted with the alternative substrate, D-galactose, by forming a hydrogen bond with the D-galactose O6, which may be the cause of the notable increase in the k_{cat} value of F280 N. In comparison, similar k_{cat} value between WT GSAI and H18T was observed. Although residue 18 of GSAI was also positioned on the binding pocket area, direct coordination between T18 and substrate was abstained, which may explain the similar value of k_{cat} before and after mutation. Nevertheless, K_m value of H18T for D-galactose was 0.4-fold lower compared with a 3.3-fold higher K_m value of F280 N. Thus, instead of improved k_{cat} value, binding affinity of H18T for D-galactose was improved. From

this point of view, both variants successfully facilitated the catalytic efficiency for D-galactose via different mechanisms.

In case of thermostability, the stability of the F280 N variant at 70 °C was lower compared with that of H18T, although both F280 N and H18T maintained their stability similarly when incubated at 60 °C and 65 °C for 60 min. The activity of F280 N was not detected after incubating at 70 °C for 40 min, whereas H18T retained its activity up to 56.4% after incubating for 60 min at 70 °C. Hence, H18T is also considered as a promising candidate for D-tagatose production although 2-fold improvement on the catalytic efficiency of H18T for D-galactose was not very high.

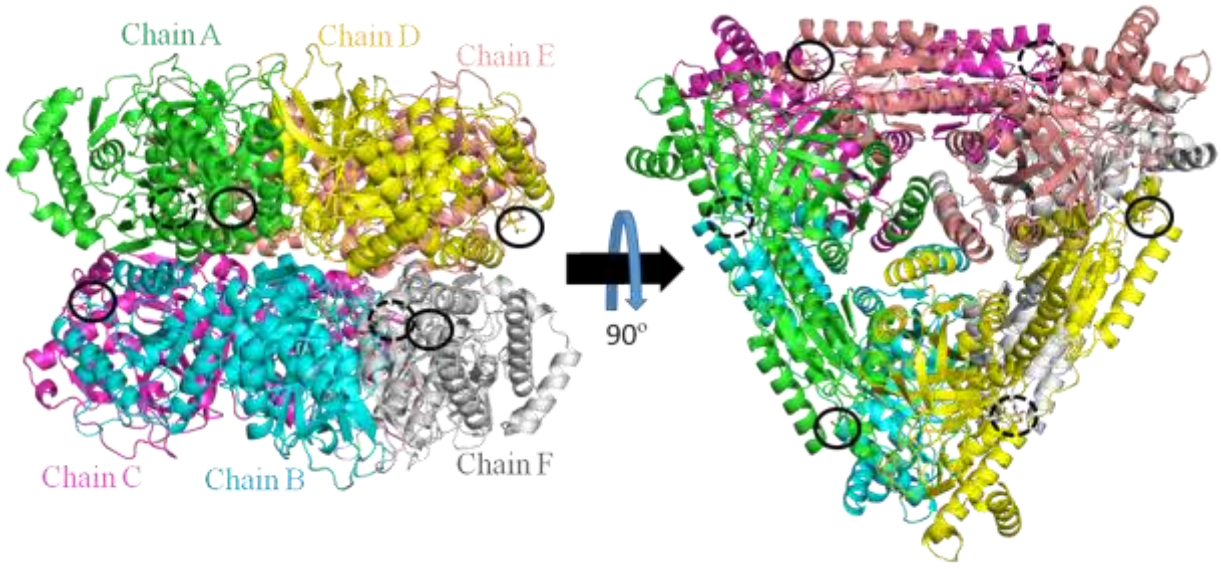

Figure II-8. Overall structure of H18T. (a) Side view and (b) top view of the hexamer structure of H18T shown with each subunit in a different color. The full black circle and the dashed black line represent the mutated residue (H18T) position at the front and back, respectively.

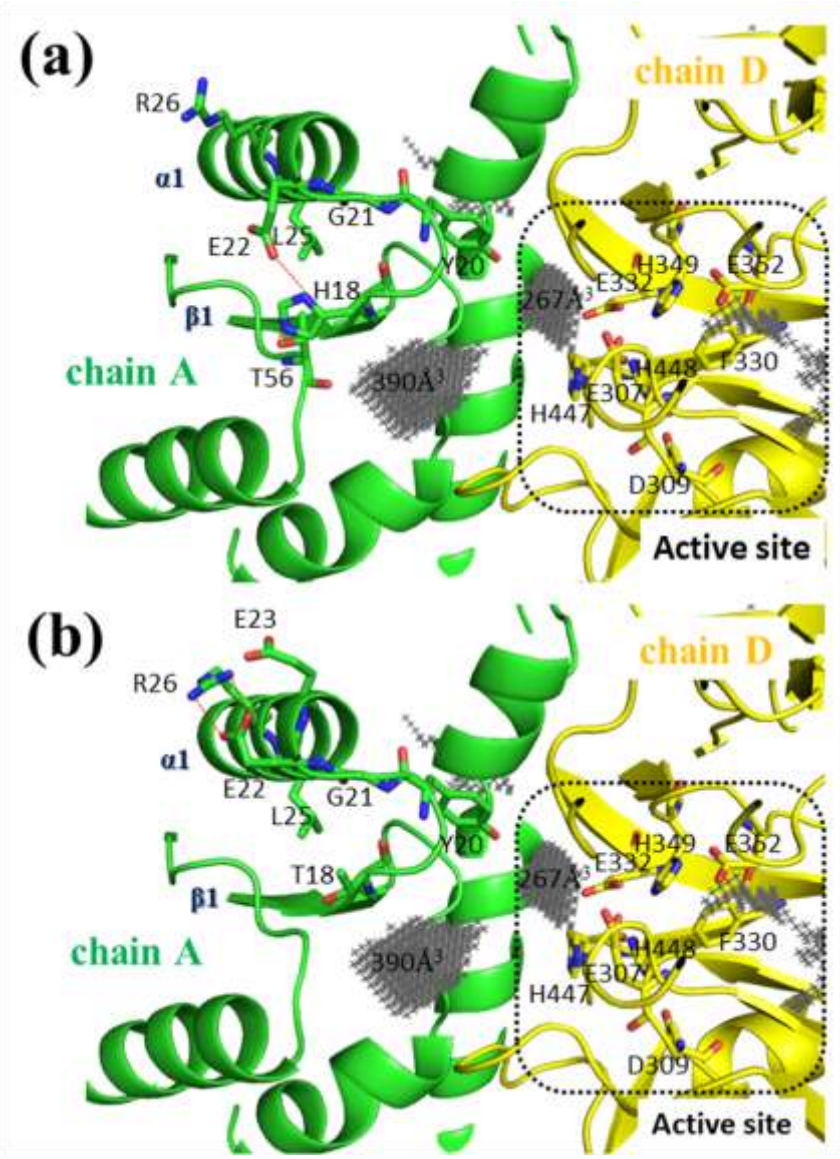

Figure II-9. Structure of the area surrounding the active site of (a) the WT GSAI and (b) H18T mutant GSAI. The gray area and the area inside the black dotted square represent the binding pocket and the active site, respectively. The red dotted lines represent the possible hydrogen bonds formed by the side chain of residue 22. Chains A and D are shown in green and yellow, respectively.

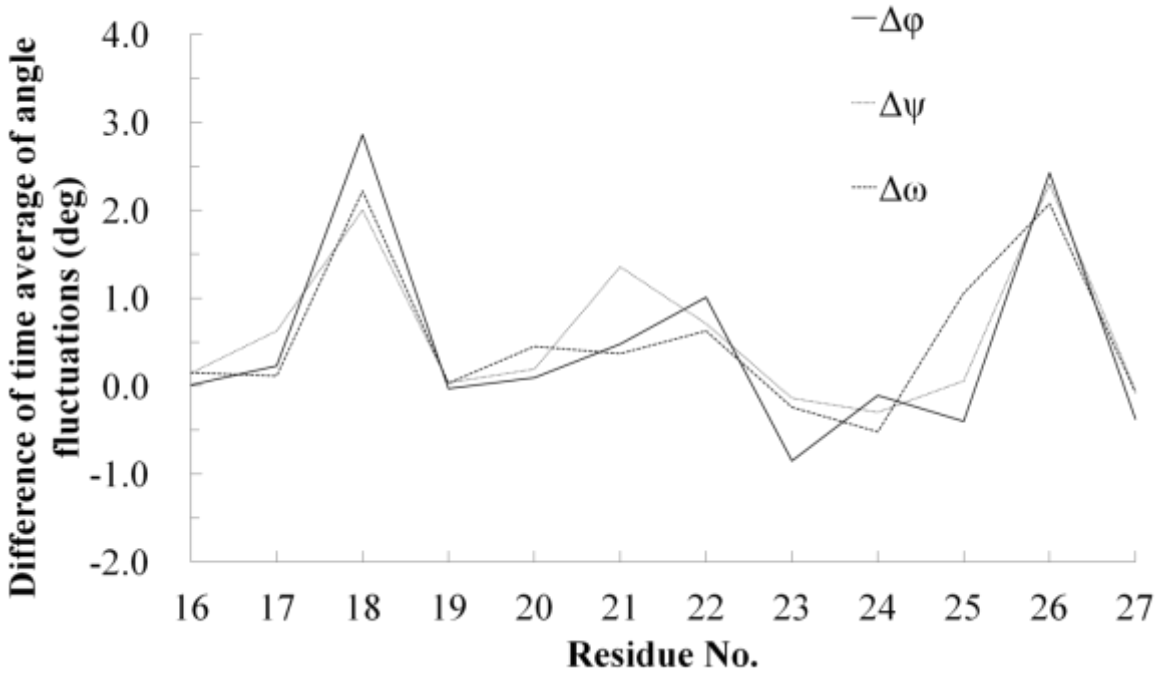

Figure II-10. Difference in angle fluctuation at residues 16–27 in the WT and H18T models. The x- and y-axis represent number of residue and difference of time average of angle fluctuations (H18T-WT), respectively. The time average of the dihedral angle fluctuation from GSAI and H18T models was calculated using the program PDBη.

Comparison-based modeling was conducted to further investigate the effect of the mutation at residue 18. The structure model of WT GSAI and H18T (Fig. II-8) was constructed with the crystal structure of L-arabitol-bound GKAI (PDB ID: 4R1Q) [25] as the template. To confirm the effect of the mutation on the size of the binding pocket, the pocket volume for both the WT and H18T models was calculated using the program POCASA [32] (Fig. II-9). For both WT and H18T, there were no alterations in the pocket volume (267 $Å^3$) around residues 307, 309, 330, 332, 349, 352, 447, and 448 at the active site and in the pocket volume (390 $Å^3$) around the mutation site (residue 18), indicating that mutation had no effect on the size of the binding pocket. Hence, we investigated the dynamical properties of the WT

and H18T models by NMA analysis. The fluctuation of dihedral angle (φ, ω, and ψ) of the whole residue of H18T was generally similar to WT. Nevertheless, a difference in the time average of dihedral angle fluctuation was detected at residues 16–27. H18T exhibited higher fluctuation, especially at positions 18, 21, 22, 25, and 26, than WT (Fig. II-10). This suggests that the structural restriction around residue 18 was reduced by H18T mutation.

Moreover, hydrogen-bonding patterns of residues 18 and 22 may be different between WT and H18T. As shown in Table II-5, the histidine residue at position 18 of WT could form four hydrogen bonds (~3.4 Å) with Y20, G21, E22, and T56. However, two hydrogen bonds with Oε1 of E22 and Oγ1 of T56 may be eliminated by changing with T18 because the positively charged side chain at residue 18 was lost by H18T mutation and then the negatively charged side chain of E22 was likely to form new hydrogen bonds (salt bridges) with the positively charged side chain of R26 (Fig. II-9). This may have caused the increased flexibility of the loop (N40–P48) between β1-α1 and the increased fluctuation of the N-terminal (S16-Q27) of α1 around the entrance of the active site of H18T. The flexibility and fluctuation around the entrance of the active site, which were important factors for improving the accessibility of the active site pocket because the accessibility could affect the intra-molecular electron transfer, substrate-binding, and catalytic activity [40], may contribute to increasing the affinity (decreasing the K_m) for D-galactose.

The addition of borate in the D-galactose isomerization reaction enhanced the production of D-tagatose (Table II-4), which was in agreement with previous reports [35, 36]. Borate favors ketoses (i.e., D-tagatose) over aldoses (i.e., D-galactose), which causes the equilibrium to shift to the production of ketoses during catalysis using L-AI and prevents the reverse reaction toward aldoses. Hence, in the presence of borate, the k_{cat} and V_{max} values of H18T and WT for D-galactose improved by 2-fold and 1.4-fold, respectively, whereas the K_m value of both WT and H18T was similar (Table II-4, Fig. II-7). However, the effect of the

addition of borate on D-tagatose production by H18T was larger than by WT. This result also suggests that the velocity constant of the reverse reaction, which in this case is the isomerization of D-tagatose to D-galactose, during catalysis using H18T may increase compared with that of WT. If the equilibrium of catalysis using H18T could shift to the production of D-tagatose, we could expect a further increase of D-tagatose yield.

Table II-5. Hydrogen bonding interactions formed by residue 18 and residue 22 in the chainA of WT GSAI and mutant GSAI (H18T) models.

Chain	No.	Residue	Atom	Distance (Å)	Atom	Residue	No.	Chain
WT GSAI								
A	18	His	O	3.0	N	Tyr	20	A
			O	3.0	N	Gly	21	
			Nδ1	2.9	Oε1	Glu	22	
			Nε2	3.0	Oγ1	Thr	56	
	22	Glu	Oε1	2.9	Nδ1	His	18	
			O	3.1	N	Leu	25	
			O	3.1	N	Arg	26	
H18T								
A	18	Thr	O	3.0	N	Tyr	20	A
			O	3.0	N	Gly	21	
	22	Glu	Oε1	3.1	N	Glu	23	
			Oε1	3.1	Oε1			
			O	3.1	N	Leu	25	
			O	3.1	N	Arg	26	
			Oε1	3.3	Nη1			
			Oε2	2.7	Nη2			

In conclusion, a potential mutant, H18T, with improved substrate specificity for D-galactose was obtained by replacing the histidine at residue 18 of GSAI with threonine. In addition, H18T showed no destabilization compared with WT. The mutation in T18 may contribute to better accessibility of D-galactose to bind at the binding pocket by increasing the structural flexibility. Therefore, we were able to show that not only the direct interaction with substrate but the accessibility of the binding pocket for substrate is also equally important for

the catalytic activity of L-arabinose isomerase. On the basis of these results, the strategy adopted by us was potentially essential for obtaining the improved substrate specificity of L-arabinose isomerase for D-galactose. A combination of H18T with the already reported variant, e.g. F280 N, or with a newly screened variant wherein the changing amino acid has a direct coordination with the substrate, D-galactose, is desired for future work. The results displayed here suggested that increased D-tagatose production can be achieved by utilizing H18T, indicating it may be valuable for industrial applications.

III.

Random mutagenesis of L-arabinose isomerase for improved activity under acidic condition

III-1. Introduction

Rational design has been extensively used to modulate functional and structural properties of proteins of interest. In contrast to rational design, irrational design using directed evolution offers the possibility to modify proteins in the absence of accurate structural and biochemical information. Error-prone polymerase chain reaction (EP-PCR) is the most common method of directed evolution approaches. By using EP-PCR, a large mutant library can be obtained for screening the desired mutants [41]. Therefore, in this study, EP-PCR was employed to obtain desirable mutant with improved stability at acidic condition because reaction under acidic condition can minimize the side Maillard reaction when done at high temperature. To dates, several attempts to reconstruct L-AI using EP-PCR have been proven successful. For example, random mutation using EP-PCR resulted in changes of the optimum pH of *Alycyclobacillus hesperidum* L-AI toward acidic condition (pH 7.0 to 6.0) [42]. However, it was not clear about the thermal stability of the above mutant, as mutation could often cause destabilization [34]. Thus, we attempted to obtain a variant L-AI possessing not only higher activity but also thermal stability under acidic condition.

In the previous result, we have obtained and characterized a mutant of *Geobacillus stearothermophilus* L-arabinose isomerase (GSAI), H18T, and shown that this mutant had greatly improved substrate specificity against D-galactose [43]. However, the activity of this mutant at low pH was found not satisfactory. EP-PCR was conducted around the binding pocket area in an attempt to increase the activity of GSAI H18T mutant at low pH, particularly at pH 6.0. The promising variant was then subjected to purification and characterization. The role of mutation in specific activity at pH 6.0 was postulated on the basis of CD analysis, kinetic parameters and structure models.

III-2. Materials and methods

III-2.1 Bacterial strains, plasmids, and medium

Escherichia coli BL21 Star (DE3) was used as a host for the random mutagenesis library and protein production. It was grown in Lysogeny Broth medium (LB) and, if necessary, 100 μg mL^{-1} ampicillin was added. The plasmid pET15b (Novagen) containing the wild-type *Geobacillus stearothermophilus* L-arabinose isomerase or its H18T mutant, namely pET15b–GSAI and pET15b–H18T, respectively, was used as an expression vector [43]. LB–ampicillin containing 0.4 % glucose was used for pre-culture of the transformant harboring an expression vector.

III-2.2 Construction of the mutant library

Error-prone PCR (EP-PCR) was performed using Diversify® PCR Random Mutagenesis Kit (Clontech Laboratories, Inc.) according to the buffer condition 5 in the manual. Namely, 640 μM $MnSO_4$ and 40 μM dGTP were added to make the buffer condition 5. EP-PCR was conducted on the area around the binding pocket of GSAI, which was divided into two regions with the first region located at residue 17–129 and the second region located at residue 186–448 (Fig. III-1). The plasmid pET15b–H18T [43] was used for the construction of the mutant library. Primers were designed in accordance with these two regions (Table III-1). The PCR cycling condition was as follows: 30 s at 94 °C, then 25 cycles of 30 s at 94 °C, 1 min at 68 °C, followed by 1 cycle of 1 min at 68 °C. The PCR products were purified using gel extraction kit (ISOSPIN Agarose Gel Kit; Nippon Gene). Megaprimer PCR of whole plasmid (MEGAWHOP) was employed for cloning of the

mutagenesis DNA using the purified EP-PCR products as a set of complementary primers and pET15b–H18T as a template. A final volume of 50 µl reaction mixture containing 1x Q5 reaction buffer, 0.2 mM dNTP, 50 ng primer, 20 ng template, and 0.02 U μl^{-1} Q5® High-Fidelity DNA Polymerase (New England Biolabs) was incubated for 1 min at 98 °C followed by 30 cycles of 50 s at 98 °C, 50 s at 60 °C, 4 min at 72 °C and 1 cycle of 4 min at 72 °C. The amplified DNA obtained from MEGAWHOP PCR was digested with *Dpn*I at 37 °C for 2 hours, transformed into *E. coli* BL21 Star (DE3) and cultured overnight at 37 °C on LB–ampicillin plate containing 0.4 % glucose.

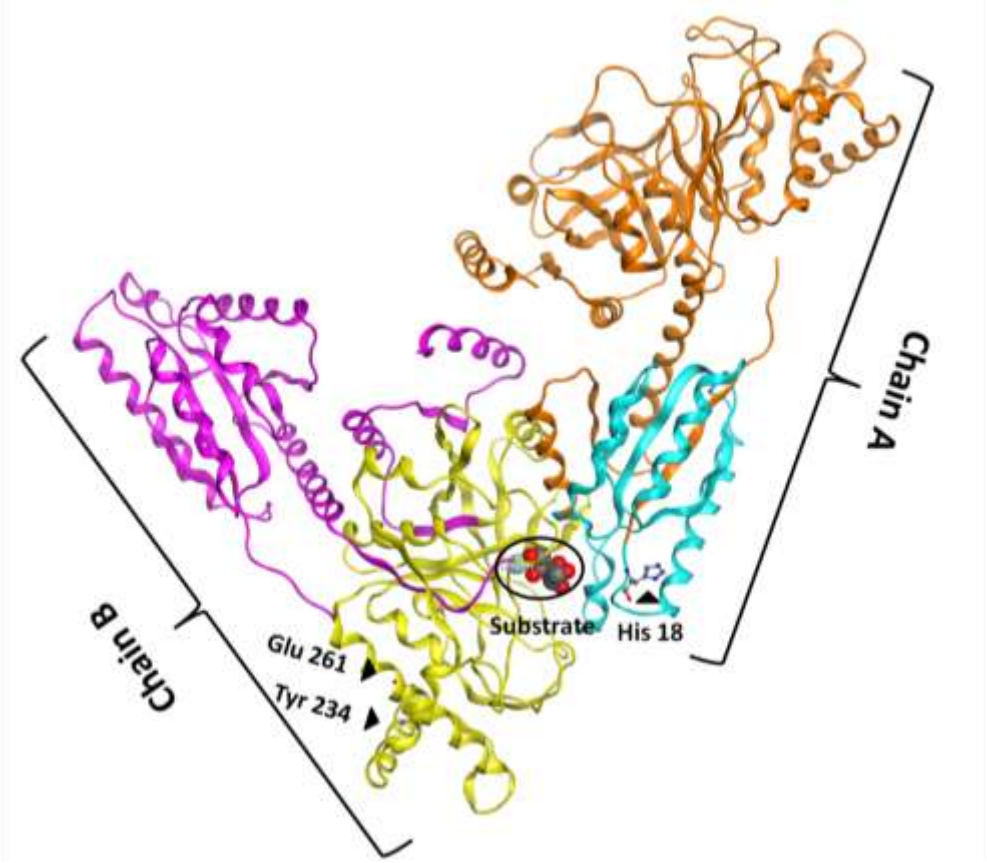

Figure III-1. Chain A and chain B of L-arabitol-bound GKAI. Residue at position 17–129 (region I) was located on chain A and shown using light blue color and residue at position 186–448 (region II) was located on chain B and shown using yellow color. Chain A and B were presented in orange and pink color, respectively. The position of His 18, Tyr 234 and Glu 261 was shown using black arrow.

Table III-1. Primers used in error-prone PCR.

Primer	Oligonucleotide sequence		Usage
	Forward (5' to 3')	Reverse (5' to 3')	
GSAI 17–129	TTTGGTTTGTAACGGGAAGC	AATCCGTATTCCCGGTCACC	Mutagenesis at residue 17–129
GSAI 186–448	TGGCTCGTTTTGGCGACAAC	ACCGCAAATGAGAAGCACGT	Mutagenesis at residue 186–448

III-2.3 Screening

Colonies grown on LB–ampicillin plate containing 0.4 % glucose were transferred to 96-well plates containing 200µl LB–ampicillin for screening. Cells were incubated at 18 °C overnight with shaking at 10,000 rpm overnight (Mix-EVR, TAITEC) and then induced by the addition of 0.2 mM IPTG for 10 h at 18 °C with shaking at 10,000 rpm. Cells were collected by centrifugation at 4,500 rpm at 4 °C for 10 min, resuspended in 42.24 µl of 50 mM McIlvaine buffer (pH 6.0), and frozen at –80°C for 1 h. Extraction of L-AI was conducted by thawing the frozen cells at 60 °C for 30 min. The mutants with improved activity at pH 6.0 were selected by measuring the activity of the extract of crude enzyme at pH 6.0. Namely, a mixture of 26.4 µl sample solution containing 2.64 µl of the above extract, 50 mM D-galactose, 1 mM $MnCl_2$, and 50 mM McIlvaine buffer (pH 6.0) was incubated at 60 °C for 30 min. After incubation, the above reaction mixture containing D-tagatose was mixed with cysteine-carbazole-sulfuric acid leading to the increasing absorbance at 560 nm [29]. This increase was followed by a Benchmark Plus™ Microplate Spectrophotometer (Bio-Rad Laboratories) at 560 nm. For further confirmation, colonies with increased activity at pH 6.0 obtained from 96-well plate screening were cultivated in 5 ml LB–ampicillin

medium. The L-AI activity of the crude cell extract at pH 6.0 was assayed and the promising mutated strain was verified by sequencing the plasmids on an ABI PRISM 3500xL Genetic Analyzer (Applied Biosystems).

III-2.4 Expression and purification of L-AI

For the simple detection and purification of L-AI, the recombinant *E. coli* BL21 Star (DE3) strains harboring the wild-type plasmid pET15b–GSAI or mutant plasmid were constructed with 6x His-Tag attached in their N termini. They were grown in LB–ampicillin medium containing 0.4 % glucose for pre-culture. A 1 % aliquot (5 ml) of the pre-culture was added to 500 mL LB–ampicillin, and the culture was incubated at 18 °C with shaking at 130 rpm. The culture was supplemented with 0.2 mM IPTG at an OD_{600} of 1.0 and the L-AI was overexpressed overnight at 18 °C with shaking at 130 rpm. Cells were harvested by centrifugation at 8000 rpm at 4 °C for 5 min and resuspended in 50 mM Tris-HCl buffer (pH 8.0). The resuspended cells were disrupted by sonication and the cell debris was removed by centrifugation at 14000 rpm at 4 °C for 15 min. The supernatant obtained was used as a crude extract. A HisTrap™ HP (1.6 x 2.5 cm; GE Healthcare) column was equilibrated with 20 mM sodium phosphate (pH 7.4) containing 20 mM imidazole. The supernatant was loaded on the column and the bound protein was eluted with a linear gradient of 20–500 mM imidazole in a 20 mM sodium phosphate buffer (pH 7.4) at a flow rate of 1 mL min^{-1}. The eluted fractions containing L-AI were further purified with a HiTrap™ Q HP (1.6 x 2.5 cm; GE Healthcare) column equilibrated with 50 mM Tris-HCl buffer (pH 8.0) and L-AI was eluted with a linear gradient of 0–500 mM NaCl in the same buffer. All purification steps were carried out using Äkta prime system (GE Healthcare). The resulting fractions were dialyzed against 50 mM Tris-HCl buffer (pH 7.5) to remove NaCl. The molecular mass of purified L-AI was

examined by sodium dodecyl sulfate polyacrylamide gel electrophoresis (SDS-PAGE) on a 10 % gel according to the method of Laemmli [27]. The protein concentration was determined using the bicinchoninic acid (BCA) method with bovine serum albumin as the protein standard [28].

III-2.5 Enzyme activity

The enzyme activities of the wild-type GSAI and the mutants were determined by measuring the amount of D-tagatose produced from D-galactose and L-ribulose produced from L-arabinose. The standard reaction mixture containing 50 mM Tris-HCl buffer (pH 8.0), 50 mM substrate, 1 mM $MnCl_2$, and 5 μg enzyme was incubated at 60 °C for 30 min and the reaction was stopped by the addition of the cysteine–carbazole–sulfuric acid mixture. As described earlier, this cysteine–carbazole–sulfuric acid solution also leads to increased absorbance at 560 nm used to quantify the amount of D-tagatose and L-arabinose generated [29]. The standard curves for D-tagatose was plotted in 50 mM Tris-HCl buffer (pH 8.0) from 0 to 0.05 μmol.

III-2.6 Effect of pH on L-AI activity

To analyze the effects of pH on L-AI activity, the pH was varied between 5.0 and 8.0 with different buffer systems. Two buffer systems, 50 mM McIlvaine buffer for pH values between 5.0 and 6.5, and 50 mM Tris-HCl buffer for pH values between 6.5 and 8.0 were used. McIlvaine buffer is composed of 0.1 M citric acid and 0.2 M disodium phosphate and has a working pH range of 2.2 to 8.0. The pH profile of L-AI activity was determined as described above using both D-galactose and L-arabinose (50 mM) as substrate. The amount of

enzyme used was 5 and 1 μg when D-galactose and L-arabinose were used as substrate, respectively.

III-2.7 Circular dichroism (CD)

To investigate the secondary structure of L-AI at pH 7.5 and 6.0, a Jasco J-715 spectropolarimeter with a Peltier cell holder and a PTC-348WI temperature controller were used to determine the far UV CD spectra of L-AI at 0.2 mg ml^{-1} in 50 mM Tris-HCl buffer (pH 7.5) and 50 mM McIlvaine buffer (pH 6.0). L-AI was dialyzed against 50 mM Tris-HCl buffer (pH 7.5) or 50 mM McIlvaine buffer (pH 6.0) overnight. The protein concentration after dialysis was measured using the bicinchoninic acid (BCA) method with bovine serum albumin as the protein standard [23]. CD measurements in 50 mM McIlvaine buffer (pH 6.0) were carried out 1 day after the determination of protein concentration. The far UV CD spectra between 205 and 250 nm were recorded using a 0.1 cm pathlength cuvette. A 10 nm min^{-1} scan rate was used with a time constant of 4 s for wavelength scans and scans were recorded five times at 1 nm intervals with a 1 nm bandwidth. The buffer spectrum was subtracted from the sample spectrum. Thermal melting was performed at 30 to 90 °C with a scan rate of 30 °C h^{-1} at 216 nm.

III-2.8 Kinetic Parameters

The kinetic parameters were determined with substrate D-galactose in 10–200 mM range for both pH conditions. The reaction mixture of buffer containing substrate and 1 mM $MnCl_2$ was incubated with 5 μg enzyme at 60 °C for 30 min. K_m (mM) and k_{cat} (min^{-1}) at pH

7.5 and pH 6.0 were calculated according to the Michaelis–Menten equation using GraphPad Prism 7 (GraphPad software).

III-2.9 Modeling and structural analysis of variant L-AIs

A Coot program was used to generate the structure model of the wild-type GSAI and H18T based on the crystal structure of GKAI from *Geobacillus kaustophilus* (PDB ID: 4R1Q) [25], which has high similarity (99 %) and high identity (97 %) with GSAI, as the template as in our previous study [43]. The structure model of the H18TY234C mutant, which involves two point mutations (H18T and Y234C), was subsequently constructed from the H18T structure. In the H18TY234C modeling, amino acid mutations were placed so that the dihedral angles of the side chain were conserved. The structural fitness of the side chain of the mutated residues was inspected using rotamer analysis by the Coot program. The rotamer probabilities of the mutated residues in the H18TY234C models were above 96.7 % (data not shown). Conformation of the variant L-AIs models was validated by Ramachandran analysis using a program Rampage [31]. The result of Ramachandran analysis for the H18TY234C models is shown in Fig. III-2. H18TY234C models have 97.4 % of the residues in the favored conformation, 2.6 % of the residues in the allowed region and no residues in the outlier region in a Ramachandran plot. Finally, the hexamer model was constructed by superimposing chain A on chains B, C, D, E, and F of 4R1Q origin using secondary-structure matching of the Coot program.

Protein dynamics information, especially the time average of the dihedral angle fluctuation, from the wild-type GSAI, H18T and H18TY234C models was derived from the elastic network model-based normal mode analysis (NMA) using the program PDBɳ [33]. Calculation of all normal modes of wild-type GSAI, H18T, and H18TY234C was performed

and the time average of the dihedral angle fluctuation was evaluated from perturbations. The pK_a values of ionizable residues for the wild-type GSAI and the mutants were calculated using the web-based program DEPTH [44].

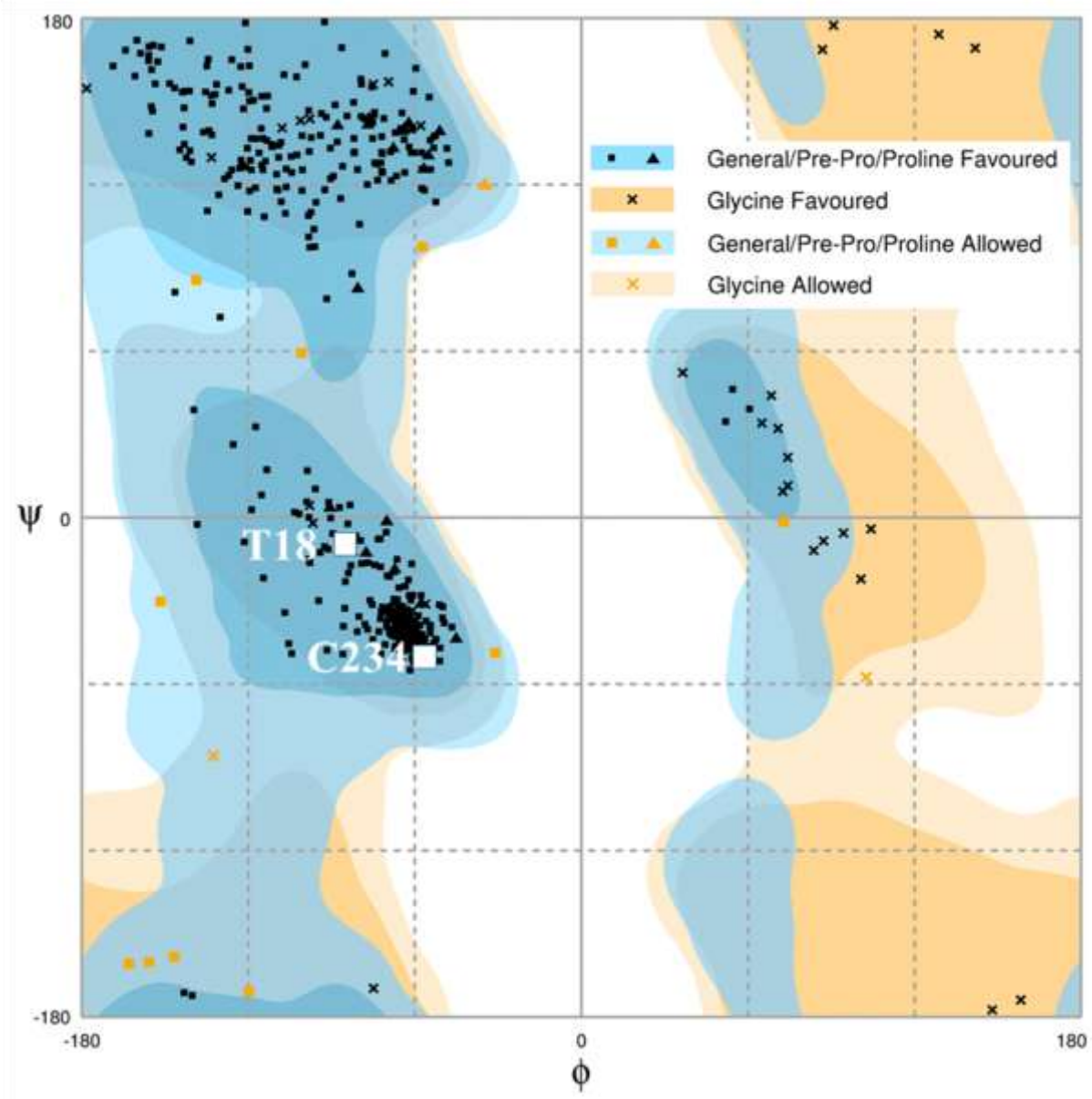

Figure III-2. Steric validation of the H18TY234C model by Ramachandran plot. The mutated residues are shown by white letters.

III-3. Results

III-3.1 Screening

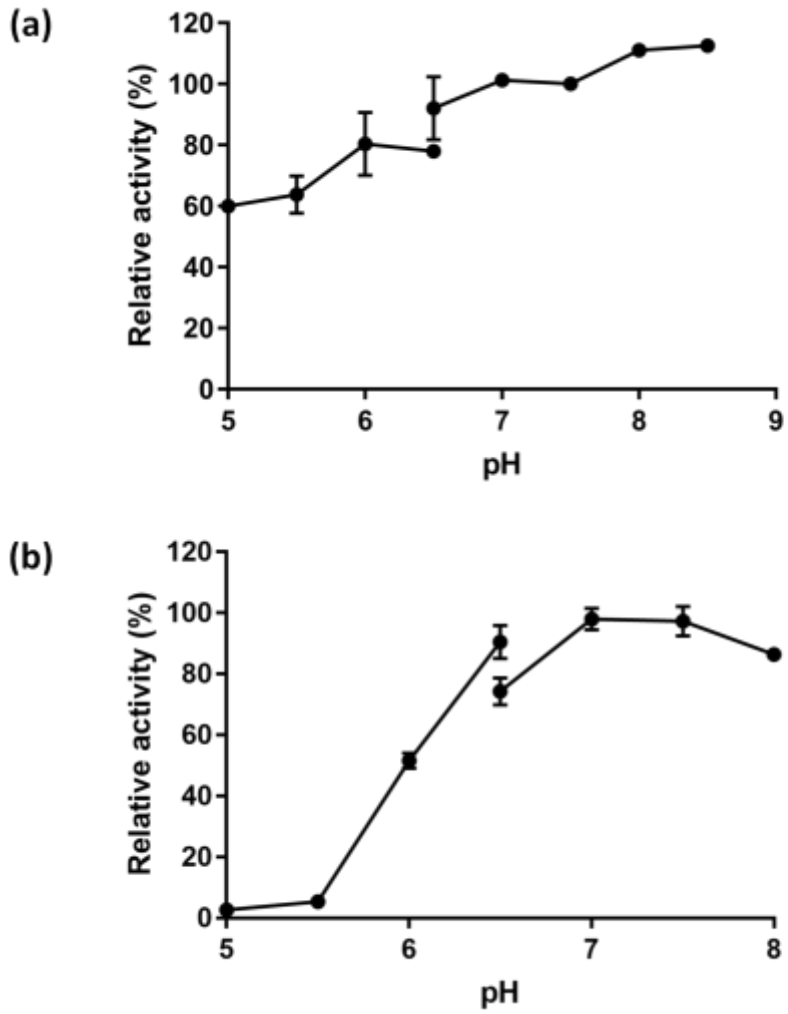

Figure III-3. Effects of pH on the stability and activity of the wild-type GSAI for L-arabinose isomerization. (a) Effect of pH on the stability of wild-type GSAI for L-arabinose isomerization. The enzyme was diluted in different buffer (pH 5.0–8.0) on ice for an hour, and the residual activities were measured in 50 mM Tris-HCl buffer (pH 8.0) containing 50 mM L-arabinose, 1 mM $MnCl_2$ after incubation at 60 °C for 30 min. (b) Effect of pH on the activity of wild-type GSAI for L-arabinose isomerization. The assay was performed in different pH buffer ranging from pH 5.0 to pH 10.0 containing 50 mM L-arabinose, 1 mM $MnCl_2$ at 60 °C for 30 min. Values are means of three replications ± standard deviation.

First, the stability of the wild-type GSAI under acidic condition was examined by incubating the enzyme at different pH values and assaying the incubated enzyme at pH 8.0. A slight decrease in activity, i.e., decrease to 60 to 80 % at pH 5.0 to 6.0, was observed (Fig. III-3A). It thus appears that the overall structure of the enzyme, including the binding pocket, is largely retained at acidic pH or regained upon pH shift to 8.0. However, the activity of GSAI at acidic condition, i.e., when the catalytic activity measurements were performed at acidic pH, decreased significantly particularly at pH 5.0 to 5.5 (Fig. III-3B). It was thus speculated that there might be a change in structure or catalytic properties around the binding pocket at low pH. A similar low activity at pH 6.0 was observed for the H18T mutant as well. On the basis of these results, we considered that instead of performing mutation on the overall structure of GSAI, mutation on the residue around binding pocket may have a greater impact on the catalytic properties of GSAI at low pH and thereby, we attempted to generate mutants of GSAI with enhanced activity at pH 6.0 using error-prone PCR around the binding pocket of GSAI.

Based on the crystal structure of GKAI (PDB ID: 4R1Q), a functional homolog of GSAI [25]. The binding pocket area was divided into two regions. First region was located at residue 17–129 on chain A and the second region was located at residue 186–448 on chain B (Fig. III-1). On the basis of this data, we attempted to create random mutation by targeting these two regions and implementation of EP-PCR on the H18T mutant [43].

Following the instruction of the EP-PCR kit used here, several different buffer conditions for EP-PCR were used to create amino acid substitution on the first region (residue 17–129) of H18T. The amounts of $MnSO_4$ and dGTP in each buffer condition were varied from 0–640 μM and 40–200 μM, respectively, according to the manual. However, the number of resultant colonies obtained after EP-PCR in the above condition was low

(approximately 300 colonies). In addition to low number of colonies, there were no variants with higher activity than the parent H18T mutant at pH 6.0. The above low colony numbers are likely due to the inhibition of *E. coli* growth when mutation was introduced in this region. In the case of random mutation at second region (residue 186–448), buffer condition 5 of the Clonetech EP-PCR manual corresponding to 640 µM $MnSO_4$ and 40 µM dGTP was used to introduce mutations. Although there were no changes in the buffer condition, we could obtain higher number of colonies (approximately 1000 colonies) than when the random mutation was conducted at residue 17–129. From these colonies, approximately 300 colonies were picked for measurement of the activities at pH 6.0. Only 3 colonies exhibited improved activity at pH 6.0 over the parent H18T mutant and were chosen for further investigation. DNA sequencing revealed 4 mutations in these 3 strain colonies on the background of H18T mutation. One strain had a mutation of E386K, second strain had a Y234C mutation and the last strain had 3 mutations with the Y234C mutation and I254F and K320T mutations.

These three colonies were grown in 5 mL of LB–ampicillin medium and the extracted enzymes were purified by Ni-affinity chromatography for further characterization. The residual activity was determined after incubation of the enzyme at 70 °C for 1 hour at neutral pH, as not only high pH 6.0 activity but also high temperature stability is important for the industrial application of GSAI. The H18TY234C and H18TE386K mutants exhibited about 100 % and 75 % residual activity of the parent H18T molecule. The last H18TY234CI254FK320T mutant had a significantly declined residual activity (Fig. III-4). Since Y234C mutation had no detrimental effect on the neutral pH stability, either I254F or K320 mutation should be responsible for the declined activity of the H18TY234CI254FK320T mutant. Thus, we generated H18TI254F and H18TK320T mutants by site-directed mutagenesis. The crude enzyme of these two mutants was purified by Ni-affinity chromatography for the following analysis. Their residual activity was similarly

examined after 70 °C incubation. No residual activity was observed for H18TI254F, whereas H18TK320T exhibited 30 % residual activity of the parent H18T (Fig. III-4). Thus, it can be concluded that the residue responsible for the declined residual activity of the H18TY234CI254FK320T mutant is Ile 254 and should be excluded for further examination.

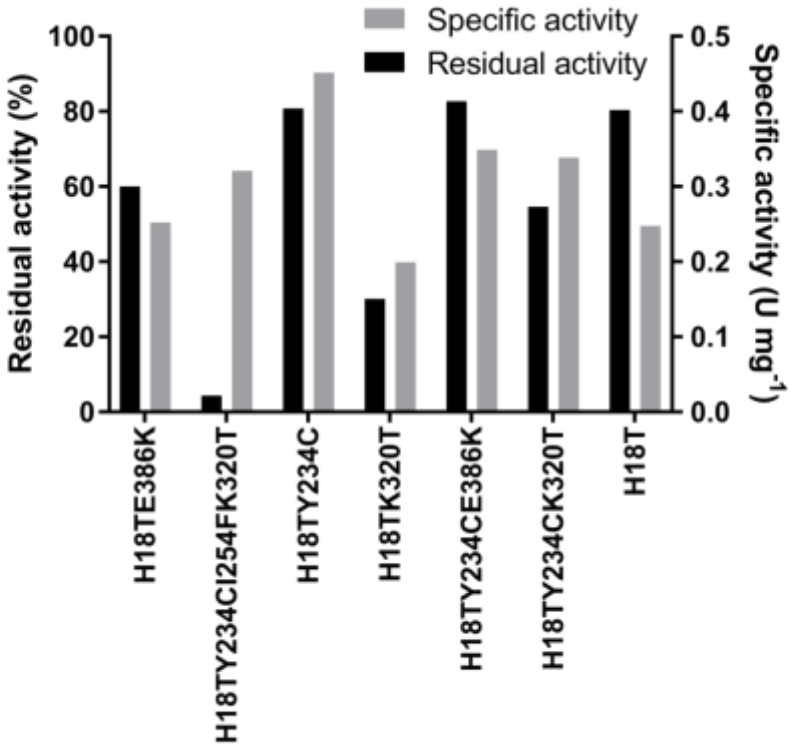

Figure III-4. Residual activity and specific activity of variant L-AIs for D-galactose isomerization. After incubation at 70 °C for 1 h, the residual activity was determined in 50 mM Tris-HCl buffer (pH 8.0) containing 50 mM D-galactose, 1 mM $MnCl_2$. Specific activity was measured in 50 mM McIlvaine buffer (pH 6.0) containing 50 mM D-galactose, 1 mM $MnCl_2$. Reactions were allowed to proceed at 60 °C for 30 min.

These four mutants, i.e., H18TY234C, the quadruple mutant, H18TE386K and H18TK320T, were then subjected to the activity assay at pH 6.0 to confirm the results of screening experiments. The H18TY234C and the quadruple mutants attained higher activities of 0.45 and 0.32 U mg^{-1} than H18T (0.25 U mg^{-1}) (Fig. III-4). However, the quadruple

mutant showed compromised residual activity upon 70 °C incubation. The H18TE386K and H18TK320T mutants showed pH 6.0 activity of 0.25 and 0.20 U mg^{-1} similar to, or even lower than, the H18T. Hence, the H18TY234C mutant turned out to be the most promising mutant in that it has a high pH 6.0 activity and 70 °C incubation stability. We then modified this H18TY234C mutant by combining E386K or K320T mutation, resulting in two new combination variants, i.e., H18TY234CE386K and H18TY234CK320T. Using the same condition as previously mentioned, these two mutants were assayed for the stability. The H18TY234CE386K mutant retained nearly the same activity as the parent H18T, whereas the H18TY234CK320T mutant lost about 30 % of the parent activity (Fig. III-4). The specific activities of both H18TY234CE386K and H18TY234CK320T at pH 6.0 were 0.35 and 0.34 U mg^{-1}, respectively, which were lower than H18TY234C (0.45 U mg^{-1}). Thus, it appears that the H18TY234C mutant without additional mutation is the most suitable variant identified so far that has enhanced activity at pH 6.0.

III-3.2 Purification and determination of effect of pH on the enzymatic properties of L-AI

To obtain a large quantity of purified proteins, *E. coli* BL21 star (DE3) was used to express the wild-type and two mutants, i.e., H18T and H18TY234C, with a 6x His-Tag at N termini in a scale-up medium, 500 mL of LB-ampicillin under the conditions described earlier. Two step purification systems were used to purify the protein from the crude extracts. The first purification step was a Ni-affinity chromatography (HisTrap^{TM} HP) followed by an ion exchange chromatography (HiTrap^{TM} Q HP). The wild-type and two mutants of GSAI obtained at each purification step were analyzed by SDS-PAGE (Fig. III-5). High purity was successfully obtained with the molecular mass at about 58 kDa, consistent with the molecular mass predicted from the amino acid sequence (Table III-2). MOE software analysis revealed

that residue 234 is located on the surface of α9 helical region of GSAI. Thus, replacing Tyr with Cys at residue 234 may result in formation of a disulfide bond between the subunits. To examine this possibility, SDS-PAGE analysis of H18TY234C in the presence and absence of β-mercaptoethanol (βME) was carried out. The H18TY234C treated with βME showed a similar size (approximately 58 kDa) to the untreated sample, indicating no formation of disulfide bonds (data not shown). Therefore, we concluded that the improvement of activity of H18TY234C at pH 6.0 is not due to the formation of disulfide bonds.

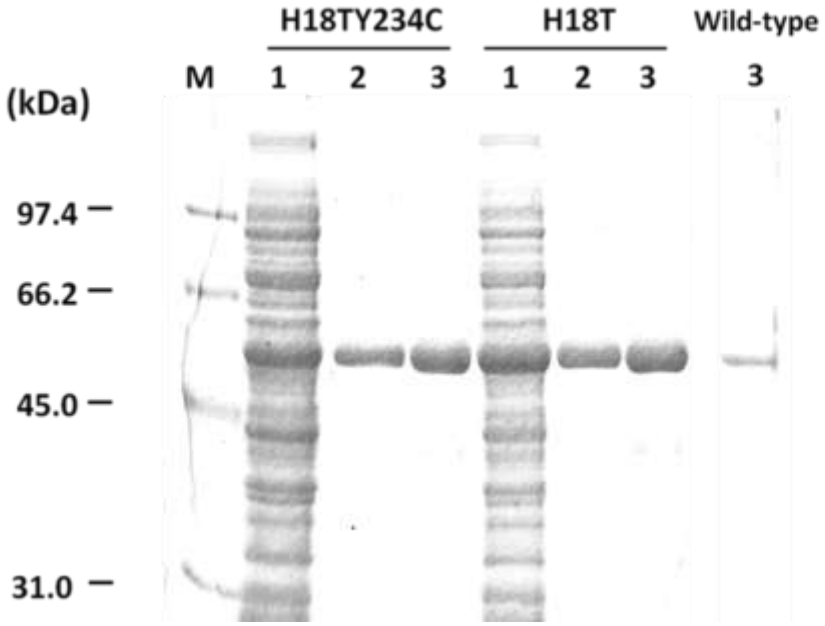

Figure III-5. SDS-PAGE analysis of variant L-AIs expressed in *E. coli* BL21 Star (DE3) using 10% acrylamide gels. Lane M, molecular weight standards; lane 1, crude cell-free extracts; lane 2, purified fraction from HisTrap™ HP chromatography; lane 3, purified fraction from HiTrap™ Q chromatography.

Table III-2. Purification of H18TY234C mutant

Purification step	Total protein (mg/ 500 ml)	H18TY234C (mg/ 500 ml)	Specific activity (U/mg)	Yield (%)
Crude homoginate[a]	239	8.10	-	100
HisTrap™ HP	8.60	5.40	0.45	66.7
HiTrap™ Q HP	3.10	3.10	0.49	38.3

[a] Protein amount of H18TY234C was determined by scanning of protein band on Coomassie blue stained SDS-PAGE.

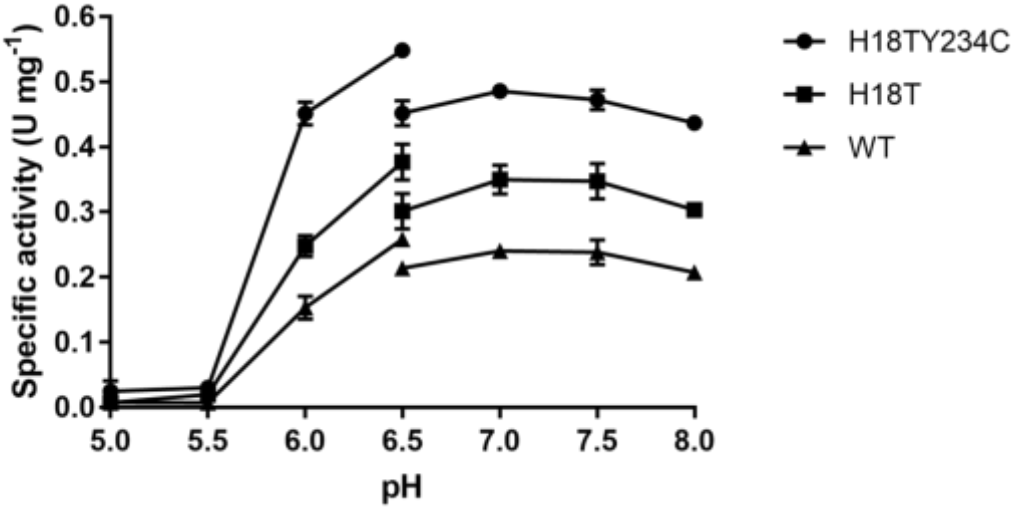

Figure III-6. Effect of pH on enzymatic activity of the variant L-AIs for D-galactose isomerization. The assay was performed in different pH buffer ranging from pH 5.0 to pH 10.0 containing 50 mM D-galactose, 1 mM $MnCl_2$ at 60 °C for 30 min. Mcllvaine buffer and Tris-HCl buffer were used for pH 5.0–6.5 and pH 6.5–8.0, respectively. Values are means of three replications ± standard deviation.

The pH profile of activity of the purified wild-type, H18T and H18TY234C was measured using D-galactose as the substrate at pH values ranging from 5.0 to 8.0. The H18T mutant showed an optimal pH range of 6.5 to 8.0, same as wild-type, but higher specific activity than wild-type by up to 1.5-fold at any pH (Fig. III-6). The improvement is caused by

higher binding affinity of the H18T mutants for D-galactose as reported previously [35]. By contrast, the optimal pH range of the double mutant, H18TY234C, was 6.0 to 8.0, demonstrating a broadened optimal pH range of activity toward lower pH. Comparison of the specific activities of H18TY234C and wild-type showed that the mutant exhibited a 3-fold higher specific activity than wild-type at pH 6.0, but only 2-fold higher specific activity at pH 6.5-8.0. This result demonstrates that Cys 234 is likely important to broaden the optimal pH range toward lower pH. Wild-type, H18T, and H18TY234C exhibited optimal activity of approximately 0.24, 0.35 and 0.48 U mg^{-1}, respectively, in the pH range 7.0–7.5 and their activity dropped sharply to almost zero when the pH was decreased to 5.5.

III-3.3 Analysis of secondary structure and thermal transition of variant L-AIs using CD spectra

The secondary structure was examined by far UV CD analysis in 50 mM Tris-HCl buffer at pH 7.5 (optimum pH condition). As shown in Fig.III-7A, the far UV CD spectrum of the H18T mutant was similar to the wild-type. On the contrary, an additional mutation at 234 onto the H18T mutant lead to a slight decrease in mean residue ellipticity, particularly around 207 nm, suggesting a slight increase in the α-helix content. The position of residue 234 within α9 helical region of GSAI may be related to the effect of the mutation at this residue on the helical content.

Since the activity of GSAI is generally decreased at low pH, the secondary structure was examined at pH 6.0 in 50 mM McIlvaine buffer at pH 6.0. As shown in Fig. III-7, the spectral shape was not a typical random coil, but had a feature of alpha/beta mix. However, the signal intensity of the wild-type was greatly diminished at pH 6.0 compared to pH 7.5, most likely due to precipitation of wild-type during a long dialysis process at pH 6.0. The

results clearly indicate unstable structure of the wild-type at pH 6.0 compared with H18T and H18TY234C. Contrary to the wild-type, the CD intensity of the H18T and H18TY234C mutants decreased at pH 6.0 compared to pH 7.5, suggesting that the secondary structure of these two mutants may have increased at pH 6.0. The overall secondary structure of the H18T and H18TY234C mutants at pH 6.0 was almost the same.

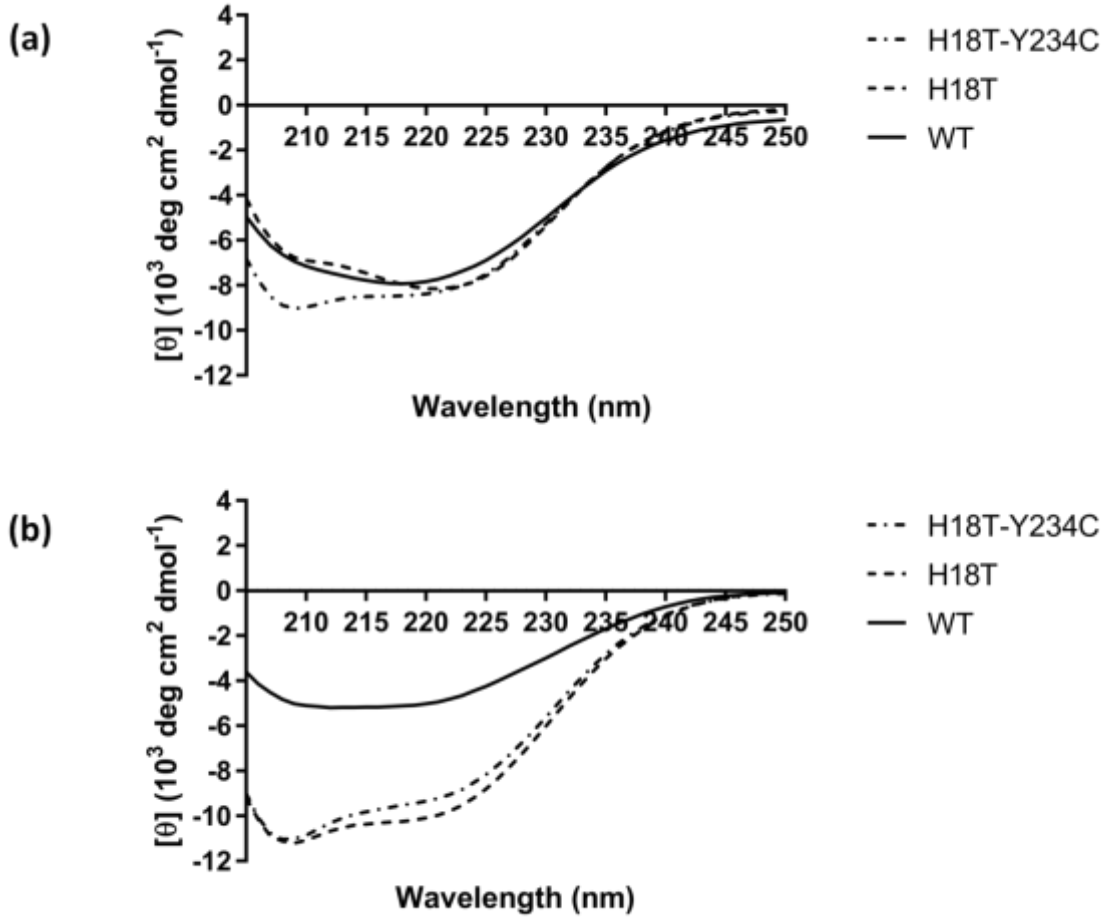

Figure III-7. Far-UV circular dichroism spectra of variant L-AIs. (a) CD curves of variant L-AIs in 50 mM Tris-HCl buffer (pH 7.5). (b) CD curves of variants L-AIs in 50 mM McIlvaine buffer (pH 6.0). The concentration of variant L-AIs was 0.2 mg ml^{-1}. CD curves were obtained by a five time accumulations.

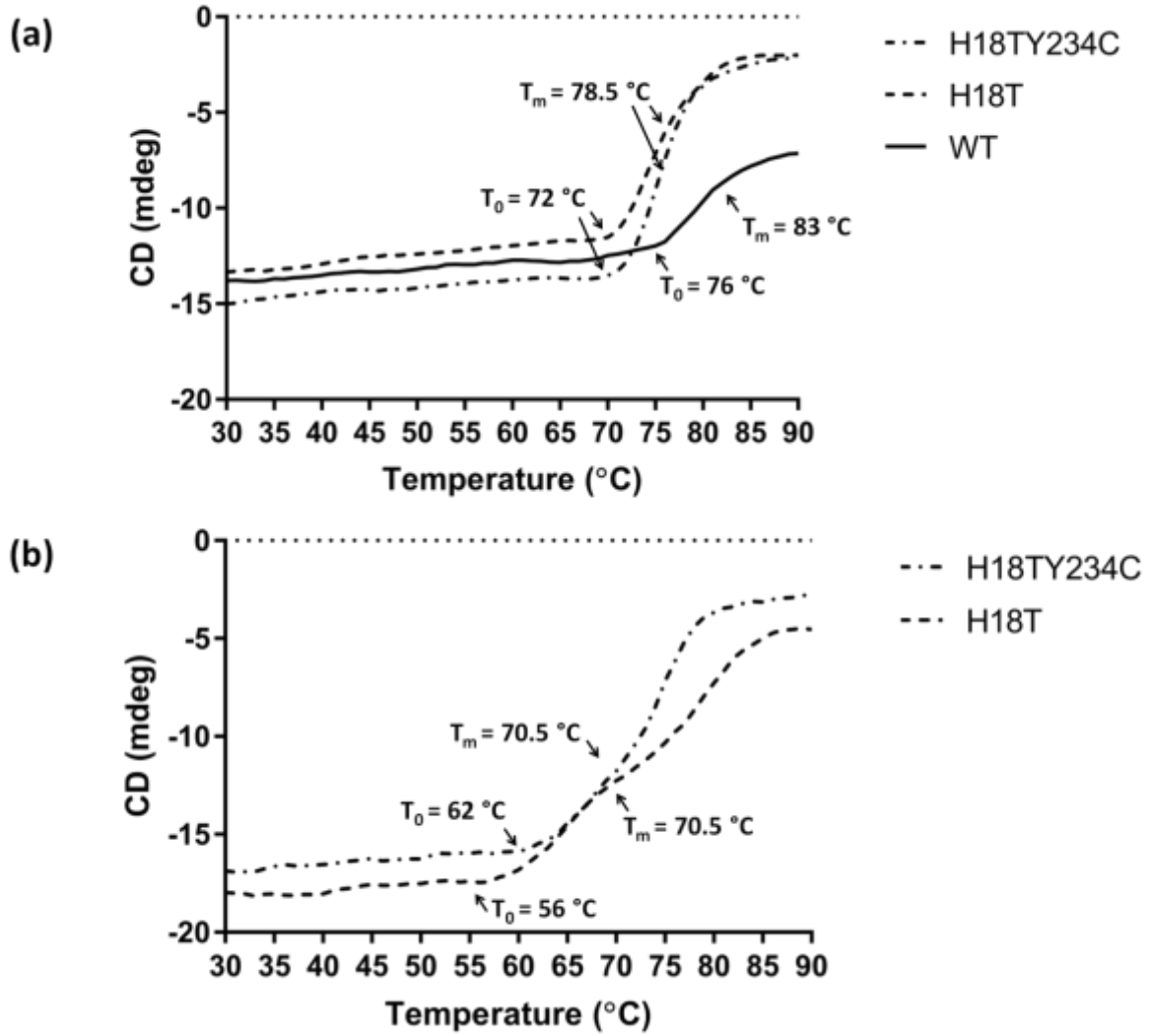

Figure III-8. **The changes in CD signal of variant L-AIs at 220 nm with temperature (30°C h^{-1}).** (a) The thermal transition of variant L-AIs in 50 mM Tris-HCl buffer (pH 7.5). (b) The thermal transition of variant L-AIs in 50 mM McIlvaine buffer (pH 6.0).

Next, the thermal denaturation was examined at pH 7.5 in 50 mM Tris-HCl. CD signal at 216 nm was used to follow structure changes. As shown in Fig.III-8A, the thermal transition of the H18TY234C mutant started at 72 °C and ended at 85 °C, identical to the H18T transition; starting and ending temperatures of these mutants were 4 °C and 5 °C lower than the wild-type. As a result, the mid-point temperature (T_m) of thermal transition of

H18TY234C and H18T was the same for each other (78.5 °C), but 4.5 °C lower than the wild-type. Nevertheless, it is evident that both mutants are stable at 60 °C, a temperature used for industrial process. The slightly decreased stability of these mutants is likely caused by mutation at residue 18. The thermal transition of the two mutants was examined in 50 mM McIlvaine buffer at pH 6.0. As shown in Fig. III-8B, the H18TY234C mutant showed a transition starting at 62 °C, 6 °C higher than that of H18T, but ending at 79 °C, 6 °C lower. Accordingly, the T_m value of the double H18TY234C mutant was 70.5 °C, same as the T_m value of the parent H18T, demonstrating that the H18TY234C mutant is also stable at pH 6.0.

III-3.4 Determination of kinetic parameters of variant L-AIs

Kinetic constants for D-galactose were assessed from Michaelis–Menten plots at pH 6.0 and the optimal pH 7.5. As shown in Table III-3, the K_m value of H18TY234C at pH 7.5 was 27.54 mM, similar to the parent H18T (31.68 mM), but the k_{cat} value of the H18TY234C mutant (34.05 min^{-1}) was slightly higher than the H18T (26.91 min^{-1}). As a result, the catalytic efficiency and specific activity of the H18TY234C mutant was higher than the parent H18T by about 1.5-fold. The kinetic constants of H18T were also determined at pH 6.0. The K_m value of H18T at pH 6.0 was 37.80 mM, higher than at pH 7.5 (31.68 mM) and the k_{cat} value at pH 6.0 was 21.39 min^{-1}, lower than at pH 7.5 (26.91 min^{-1}), resulting in slightly decreased catalytic efficiency and specific activity of H18T at pH 6.0 compared to pH 7.5. Similar to the parent H18T, the k_{cat} value of the H18TY234C mutant also decreased at pH 6.0 (30.91 min^{-1}) compared with pH 7.5 (34.05 min^{-1}). Unlike the parent H18T, however, a slight decrease in K_m value at pH 6.0 (22.41 mM) was observed for H18TY234C compared with the K_m value at pH 7.5 (27.54 mM), indicating that the binding affinity for D-galactose at pH 6.0 increased by mutation at residue 234 in HT18TY234C. Subsequently, the

decrease of both K_m and k_{cat} rendered the catalytic efficiency and specific activity of the double H18TY234C mutant little change at pH 6.0.

Table III-3. Kinetic parameters of variant L-AIs at pH 7.5 and 6.0.

GSAI	pH 7.5				pH 6.0			
	Specific activity ($U\ mg^{-1}$)	K_m (mM)	k_{cat} (min^{-1})	k_{cat}/K_m ($mM^{-1}\ min^{-1}$)	Specific activity ($U\ mg^{-1}$)	K_m (mM)	k_{cat} (min^{-1})	k_{cat}/K_m ($mM^{-1}\ min^{-1}$)
H18T	0.32	31.7	26.9	0.85	0.23	37.8	21.4	0.57
H18TY234C	0.44	27.5	34.1	1.24	0.42	22.4	30.9	1.38

(n=3)

III-4. Discussion

In recent years, a growing attention is directed to D-tagatose, a natural low calorie sweetener that has great potential to replace sucrose. D-tagatose possesses similar characteristics with sucrose in term of taste and degree of sweetness [4, 5]. To produce D-tagatose, an enzymatic pathway using L-arabinose isomerase as the catalyst and D-galactose as the substrate has been a more preferable approach than a chemical process that has complicated process and formation of undesirable by-products.

We have previously reported a mutant, H18T, of GSAI that was generated using site-directed mutagenesis. This mutant exhibited increased substrate specificity for D-galactose and showed no changes in stability, but diminished activity at pH 6.0 [43]. In this study, random mutation using error-prone PCR was used to improve the activity of GSAI at pH 6.0 by using H18T as the template. A mutation at residue 234 from Tyr to Cys was found to have the highest improvement on the activity of GSAI at pH 6.0. A double mutant containing both H18T and Y234C mutations, i.e., H18TY234C, maintained the stability similarly to the parent H18T molecule and acquired improved activity at pH 6.0. Its optimal range broadened toward pH 6.0 and the specific activity at pH 6.0 was 3- and 1.8-fold higher than wild-type and H18T, respectively (Fig. III-6).

It has been shown that a different type of mutants also improves the acidic adaptation of L-AI. For example, the optimal pH of Q268KN175H derived from *Bacillus stearothermophillus* US100 L-AI shifted from 7.5–8.0 to 6.0–6.5 upon replacing Gln with Lys at residue 268 [45]. Recently, a similar work was presented by Xu et al. [16] that substituting Asp at residue 268, 269, and 299 of *Lactobacillus fermentum* CGMCC2921 L-AI (LFAI) with Lys resulted in altering the optimum pH and a combination of three substitutions, which was identified as D268KD269KD299K, shifted optimum pH from 6.5 to 5.0. In

addition, this D268KD269KD299K mutant achieved 2.3-fold higher activity at pH 5.0 than wild type at the same pH. On the other hand, the H18TY234C achieved 3-fold higher activity at pH 6.0 than the wild type protein, although it showed no activity at pH 5.5. Although less active than D268KD269KD299K at pH 5.5, the H18TY234C is still a suitable candidate for D-tagatose production when carried out at pH 6.0.

We further investigated the role the Tyr 234 plays in GSAI in improving the activity of the enzyme. The specific activity, shown in Fig. III-6, of the H18TY234C mutant was generally enhanced at all pH range (pH 6.0–8.0) compared with the parent H18T protein and the wild-type. The highest improvement was seen at pH 6.0, thereby broadening the optimal pH range toward acidic condition. It appears that k_{cat} may play a key role in general activity improvement of H18TY234C, because its k_{cat} value at pH 7.5 increased while retaining the K_m of H18T. When the kinetic parameters at pH 6.0 were compared with pH 7.5, the H18T showed decreased k_{cat} value and increased K_m value (reduced affinity) at pH 6.0, and the H18TY234C showed only decreased k_{cat} value at pH 6.0. The decreased k_{cat} may be due more or less to instability at pH 6.0 similarly to the H18T. The H18TY234C showed decreased K_m (i.e., improved affinity), different from the value for H18T at pH 6.0. As such, the improvement of affinity at pH 6.0 may be related to the change in the binding pocket area when Tyr was replaced with Cys at residue 234. Thus, we can infer that while k_{cat} was simply responsible for the higher activity of H18TY234C at pH 6.5–8.0, it seemed that the improvement at pH 6.0 was likely caused by K_m.

The possible cause of the change in the binding pocket area was examined by constructing the structure model of H18TY234C (Fig. III-9). Such analysis revealed that a mutation from a bulky aromatic amino acid, Tyr, to a smaller amino acid, Cys, leads to an increase in the size of cavity volume around residue 234 by 294±68 $Å^3$ (Fig. III-10A). The mutation into Cys also impacted the dynamical properties of GSAI, particularly in the area

near residue 234. Difference in time average of dihedral angle fluctuation was seen at residue 229–236 (Fig. III-10B). The H18TY234C mutations provided higher fluctuation at residue 229-236 than the H18T with the highest enhancement detected at residue 234. This result was indicative of the reduction by Y234C mutation of the structural restriction. Although residue 234 is located far from the active site, previous studies have suggested that mutation at both proximal and distal residue can affect the catalytic rate due to conformational and dynamic changes that are reflected on the active site [47, 48]. Thus, we propose that increasing the size of cavity volume and the flexibility may contribute to altering the condition of the binding pocket area of GSAI via protein motion, thereby possibly resulting in increased specific activity of the H18TY234C mutant.

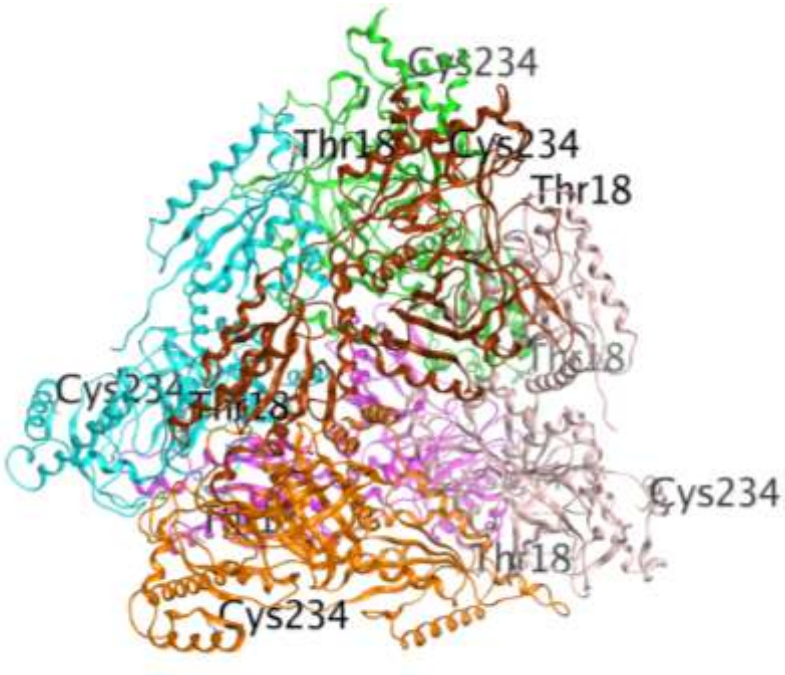

Figure III-9. The overall structure of H18T-Y234C. The hexamer structure of H18T-Y234C was constructed using *Coot* program. Mutated positions are shown as stick and are labeled.

It should be noted that the overall structure of the H18TY234C mutant model was almost conserved even if the modeling program was changed. For example, RMSDs of

overall structures between H18TY234C models generated by *Coot* and *Rosetta* (the web-based version of this program is currently offered as *Robetta*; http://new.robetta.org/) were 0.5 Å for Cα atoms and 1.2 Å for all atoms, respectively. Moreover, the structure around Y234C mutation site in the H18TY234C mutant model was also almost conserved. RMSDs around Y234C (229-236th residues) in the models generated by *Coot* and *Rosetta* were 0.3 Å for Cα atoms and 1.1 Å for all atoms, respectively.

Computational investigation on the pK_a value of surrounding residue using DEPTH software was conducted to provide further insight into the effect of mutation on the environments surrounding residue 234 at pH 6.0. In comparison with wild-type and H18T, an increase of the predicted pK_a value of Glu 261 for H18TY234C, which is positioned at the opposite side of residue 234 (Fig. III-10C), was detected by up to 0.2 pH unit. However, it is unlikely that the pK_a shift directly implicates its effect on the binding pocket area because residue 261 is located far away from the active site. The change in pK_a value may alter the interaction between the residue 261 and the surrounding residues and then may cause the change in the quaternary structure of GSAI and thereby, indirectly change the environment of binding pocket area. Information about the crystal structure of wild-type, H18T and H18TY234C is required to reveal in detail how mutation at residue 234 from tyrosine to cysteine can contribute to the enhanced activity at pH 6.0.

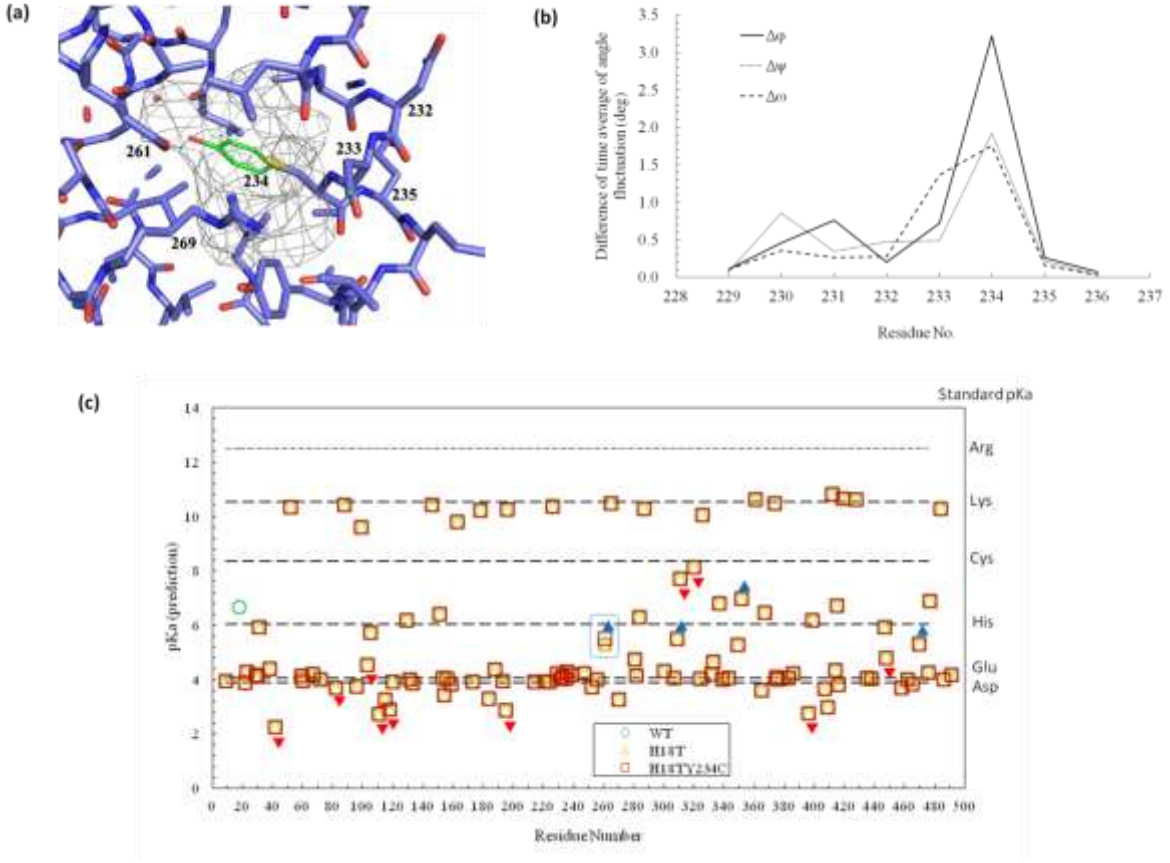

Figure III-10. Effects of mutation at residue 234. (a) Effect on pocket volume around residue 234. Tyrosine (green) and cysteine (blue) residue was superimposed at position 234. A pocket is displayed as a grey mesh. (b) Difference in angle fluctuation at residue 229–236 in the H18T and H18TY234C models. The x- and y-axis represent number of residue and difference of time average of angle fluctuation, respectively. Positive values of Δφ, Δψ and Δω indicate the increase in the fluctuation due to the Y234C mutation. (c) Comparison of pK_a value between wild-type, H18T and H18TY234C. Upward triangle in blue color represents the residue that is expected to have pK_a higher by 1 pH unit or more than standard. Downward triangle in red color represents the residue that is expected to have pK_a lower by 1 pH unit or more than standard.

In conclusion, directed evolution using error-prone PCR has been utilized to improve the pH tolerance at low pH condition (pH 6.0). A variant L-AI, H18TY234C, with increased activity at pH 6.0 was successfully obtained and this variant showed a broader optimal pH range of 6.0–8.0 and a 3-fold higher activity at pH 6.0 than the wild type. In addition, the H18TY234C mutant exhibited no destabilization after mutation. Therefore, this H18TY234C mutant that possessed both thermostability and improved activity at pH 6.0 may be a promising and suitable candidate for D-tagatose production.

IV

Expression, Folding, and Activation of Halophilic Alkaline Phosphatase in Non-Halophilic *Brevibacillus choshinensis*

IV-1. Introduction

Halophilic enzymes easily degrade when used for industrial application compared with thermophilic and alkaliphilic enzymes because of their instability in low-salt environments. Thus, the study on the stabilization and folding mechanism of halophilic enzymes is necessary for the industrial application of halophilic enzyme. In this study, Alkaline phosphatase (ALPase) from *Halomonas* sp.593 was used. ALPase is a periplasmic enzyme that has been well studied in other Gram-negative bacteria [49–52]. ALPases from extremely halophilic archaea have also been widely reported [53–57], but the well-studied ALPases from moderately halophilic bacteria have been restricted to *Vibrio* [58–60] and *Halomonas* species [23, 24, 61]. Hence, a detailed study of the ALPases from moderately halophilic bacteria should boost our understanding of the stability and folding mechanism of halophilic proteins under high salt conditions. Although most bacterial ALPases containing our HaALPase, *Halomonas* ALPase, form a dimer [51, 52, 61], the ALPases from psychrophilic marine *Vibrio* sp. and *V. cholerae* have been reported to be monomeric [59, 60].

Halophilic enzymes have many acidic amino acids on their surface, and the associated strong electrostatic repulsion leads to their denaturation under low-salt conditions [62–65]. The addition of salt reduces unfavorable electrostatic free energy, leading to the enhancement of protein folding and enzymatic activity via its electrostatic effects as well as effects on hydrophobic interactions [64]. In addition, a high salt concentration is necessary for halophilic enzyme stabilization because of the binding of salt to specific sites on the surface of the folded polypeptide. In the case of halophilic malate dehydrogenase from *Haloarcula marismortui*, it was reported that there are specific ion binding sites, particularly four strong chloride-binding sites at the dimer–dimer interface of the tetrameric enzyme [66–68].

We hypothesized that these are specific Na^+ binding sites for the activation of HaALP [23]. However, further discussions are needed to clarify the stabilization mechanism of halophilic enzymes.

In this study, we discussed the effects of salts on HaALP using the *Brevibacillus choshinensis* expression system. *B. choshinensis* is Gram-positive and can secrete proteins in culture medium. We successfully obtained the active form of HaALP using this expression system in order to study this enzyme. Then, we attempted to study the refolding of HaALP in detail. To distinguish the effects of salts on hydrophobic interactions from electrostatic effects or ionic binding, the non-ionic osmolyte trimethylamine N-oxide (TMAO) was used to refold HaALP. The effect of TMAO is due to thermodynamic interactions with proteins rather than binding [69]: TMAO is preferentially excluded from the protein surface, which leads to thermodynamic stabilization of the protein in its native state. Using TMAO as a non-ionic osmolyte in this study distinguished the effects of salts on hydrophobic interactions from electrostatic effects or ionic binding and enabled us to study the role of Na^+ ions in HaALP refolding.

IV-2. Materials and methods

IV-2.1 Bacterial Strains and Culture

For cloning and expression of the *haalp* gene, *Escherichia coli* JM109 and *B. choshinensis* HPD31-SP3 (FERM BP-8479) were used in LB-ampicillin and TM-neomycin media [70], respectively. Transformants were grown at 30 °C for 2 days with shaking at 160 rpm.

IV-2.2 Secretory Expression of HaALP by *B. choshinensis* and Purification

The DNA fragment encoding the HaALP mature region was amplified by PCR using pHA [23] as template DNA. The ALP-bre-F primer (5′-AgT TCC gCA TTC gCT gCC gAg gTC AAg AAC gTg-3′) and ALP-bre-R primer (5′-CAT CCT gTT AAg CTT CAC TCg ACC AgC gAC TTg-3′) were used. HaALP consisted of a pre-sequence of 29 amino acids (MTFCMKQKTAVGSLVGGMLLASVAVPASA) and a 497-amino-acid-long mature sequence (MW 54110.81) [23]. The mature HaALP region and the linearized pBIC3 vector were mixed and then transformed into host *B. choshinensis* to form the construct pBIC3HaALP using the BIC System (Takara). For constructing the His-tagged version of HaALP, PCR was performed using pNA [23] as a template and the HisHaALP F primer (5′-gCA TTC gCT gCA gAT CAT CAT CAT CAT CAT CAC AgC-3′) and ALP-bre-R primer (5′-CAT CCT gTT AAg CTT CAC TCg ACC AgC gAC TTg-3′). The His-tagged mature HaALP region and the linearized pBIC3 vector were mixed and then transformed into the host to construct the pBIC3HisHaALP plasmid.

Brevibacillus choshinensis colonies harboring either the pBIC3HaALP or the pBIC3HisHaALP plasmid were directly grown in 10 mL × 10 (total 100 mL) TMNm nutrient medium containing 0 or 0.2 M NaCl at 30 °C for 48 h.

For pBIC3HaALP, the collected medium (100 mL) was applied to a HiTrap Q HP (1.6 cm × 2.5 cm; GE Healthcare) using an Akta prime chromatography system (Amersham, USA). The bound proteins were eluted with 100 mL of a linear gradient of NaCl from 0.2 to 0.7 M in 50 mM Tris–HCl (pH 8.0) and 2 mM $MgCl_2$. For pBIC3HisHaALP, the collected medium was first applied to a HisTrap HP (1.6 cm × 2.5 cm; GE Healthcare) with a linear gradient of imidazole from 20 to 500 mM in 20 mM Na–phosphate buffer (pH 7.5) and 2 mM $MgCl_2$, containing 0.2 M NaCl, and then, the pooled fraction containing HaALP was digested by 0.1 U thrombin/1 μg HaALP (Wako; 9002-04-4) at 18 °C overnight. Next, the digested sample was applied to a HiTrap Q HP in a similar manner as that for the pBIC3HaALP.

Fractions containing HaALP were pooled and dialyzed against 50 mM Tris–HCl (pH 8.0) and 2 mM $MgCl_2$ containing 0.4 M NaCl. To confirm purity, 10% (or 8%) SDS-PAGE was performed in accordance with the Laemmli method [27]. Gels were stained using Coomassie brilliant blue. The amount of protein was measured using the BCA method as described by Smith et al. [28].

IV-2.3 HaALP Activity Assay

HaALP activity was assayed as described previously [23]. The increase in absorbance at 405 nm was monitored at 37 °C in a reaction mixture containing 0.97 M diethanolamine buffer (pH 10.25), 0.25 mM $MgCl_2$, and 10 mM p-nitrophenylphosphate. One unit was defined as the rate of formation of 1 μmole product/min.

IV-2.4 Refolding Assay and Structure Evaluation

Samples (0.5 mg/mL) were dialyzed against 50 mM Tris–HCl (pH 8.0) containing 6 M urea at 4 °C overnight and then dialyzed against 50 mM Tris–HCl (pH 8.0), 2 mM $MgCl_2$, and 5 mM DTT for 6 h to remove urea. The dialyzed samples were normalized to 0.4 mg/mL, and then, aliquots (5 μL) were diluted with 45 μL of different salt solutions (final concentration: 0–3 M) or with 3 M TMAO solution in a refolding buffer [100 mM diethanolamine (pH 8.0) and 2 mM $MgCl_2$]. Samples were kept at 4 °C, and activity was assayed daily. For structure evaluation, refolded samples were subjected to native PAGE. Native PAGE was performed using 10% polyacrylamide gels at 4 °C in accordance with the Laemmli method [27] without SDS. The area (the relative amount of protein) in the band stained with Silver Stain KANTO III (Kanto Chemical Co., Inc.) was measured using ImageJ software (National Institutes of Health, USA).

IV-3. Results

IV-3.1 Secretory Expression of HaALP and Purification

We previously attempted to express halophilic HaALP in non-halophilic *E. coli* BL21 Star (DE3) pLysS. However, the expressed HaALP showed little activity and required refolding in 3 M NaCl for activation [23]. We need to achieve more active HaALP to study its stabilization and folding mechanisms. HaALP is a periplasmic enzyme. Therefore, nonhalophilic *B. choshinensis* was used to express halophilic HaALP. This gram-positive bacterium has been used for the efficient production of a variety of recombinant proteins, especially secretory ones [71, 72]. Hence, this host can also be expected to efficiently express periplasmic proteins such as HaALP. It was further genetically improved by deleting a spore-forming gene, *spoIIAC*, and two secretory protease genes, *imp* and *emp* [72].

Table IV-1. Summary of purification via HiTrap Q HP of HaALP expressed in culture medium in the absence of NaCl

Fractions	Total protein (mg)	Total activity (U)	Specific activity (U mg^{-1})	Fold	Yield (%)
Culture supernatant	2670	16000	6.00	1.00	100
lane 6-10	66.0	66.0	1.00	0.19	2.00
lane 11-16	27.0	324	12.0	2.00	1.00
lane 17-18	5.00	16800	5600	934	0.10

For HaALP purification, 100 mL of culture supernatant was used

First, we attempted to express HaALP without a His-tag because we could not express it with a His-tag in *E. coli* [23]. As shown in Fig. IV-1, an abundance of HaALP, the molecular weight of which was estimated to be about 54 kDa by SDS-PAGE, was found in the culture supernatant compared with the case in the control (no expression vector), suggesting that HaALP was successfully expressed and secreted. HaALP was purified via

HiTrap Q HP, and its purity was confirmed by SDS-PAGE. Figure IV-2A shows three fractions (lanes 6–10, lanes 11–16, and lanes 17 and 18) of HaALP. The associated specific activities were 1, 12, and 5603 U/mg, respectively (Table IV-1). To predict the structure, native PAGE was performed. The results showed that lanes 6–10 contained S1, S2, and S3 structures, lanes 11–16 contained the S2 structure, and lanes 17 and 18 contained the S4 structure (Fig. IV-2B). We previously reported that S1 and S2 were non-reversible denaturation structures; S3 was the monomer precursor (folding intermediate), which was estimated to be about 45 kDa from gel filtration, of the active dimer structure (108 kDa); and S4 was the active dimer structure, which was estimated to be about 86 kDa from gel filtration. Only S4 was positive in activity staining [23]. In this study, S4 was secreted using *B. choshinensis*. The amount of active HaALP was about 5 mg in 100 mL of medium (Table IV-1). Because there was an abundance of HaALP without activity found amidst active HaALP, 0.2 M NaCl was added to the culture medium to stabilize HaALP, and HaALP was purified in a similar manner as mentioned previously. In a medium containing 0.4 M NaCl, *B. choshinensis* growth was inhibited (data not shown). As shown in Fig. IV-3, there was almost no HaALP in lanes 6–10, whereas presumably S4 HaALP increased in lanes 15–17. The HaALP activities of the two fractions (lanes 11–14 and lanes 15–17) were 208 and 5598 U/mg, respectively (Table IV-2). Thus, we could achieve active HaALP at a yield of about 12 mg in 100 mL of medium.

Table IV-2. Summary of purification via HiTrap Q HP of HaALP expressed in culture medium containing 0.2 M NaCl

Fractions	Total protein (mg)	Total activity (U)	Specific activity (U mg^{-1})	Fold	Yield (%)
Culture supernatant	2460	71300	29.0	1.00	100
lane 6-10	-	-	-	-	-
lane 11-14	7.00	651	208	3.00	0.30
lane 15-17	12.0	63400	5590	182	0.40

For HaALP purification, 100 mL of culture supernatant was used

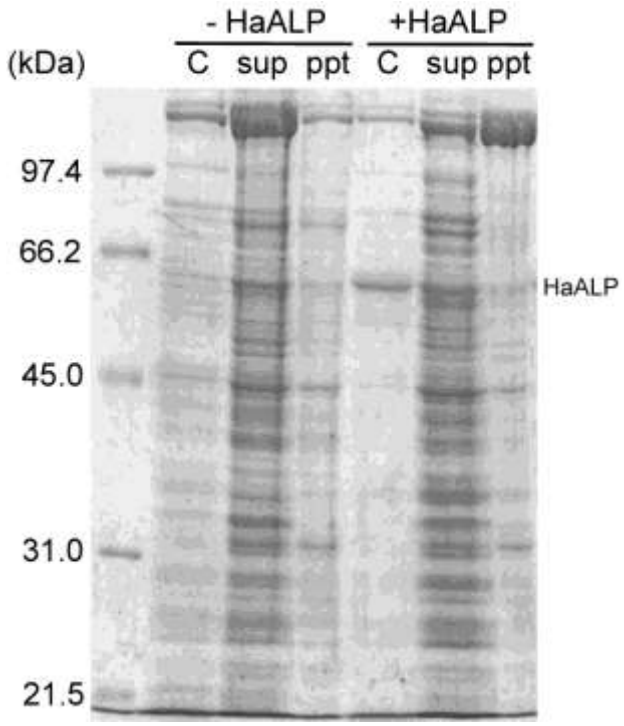

Fig. IV-1 Expression and secretion of HaALP in *B. chosinensis*. Cells were grown in 5 ml culture medium at 30°C for 3 days. −HaALP, control (no expression vectors); +HaALP, pBIC3HaALP; C, culture supernatant; sup, supernatant of disrupted cells; ppt, precipitate of disrupted cells. HaALP shown next to the far-right lane indicates the mobility in 10% SDS-PAGE.

Next, we attempted to express HaALP with a His-tag in *B. choshinensis* to increase its purity. Active His-tagged HaALP was also secreted using *B. choshinensis* in 0.2 M NaCl. We finally succeeded in achieving active His-tagged HaALP using *B. choshinensis*. As shown in Fig. IV-4, HaALP appeared to be highly purified, with more than 95% purity as determined by two-step chromatography, with a size of about 56 kDa. A summary of the purification is presented in Table IV-3. HaALP was obtained at a yield of 3.2 mg in 100 mL of medium, with a specific activity of 6679 U/mg. This value is in close agreement with the previously

determined specific activity of HaALP of approximately 6700 U/mg [24]. This highly pure HaALP was used in the folding experiments.

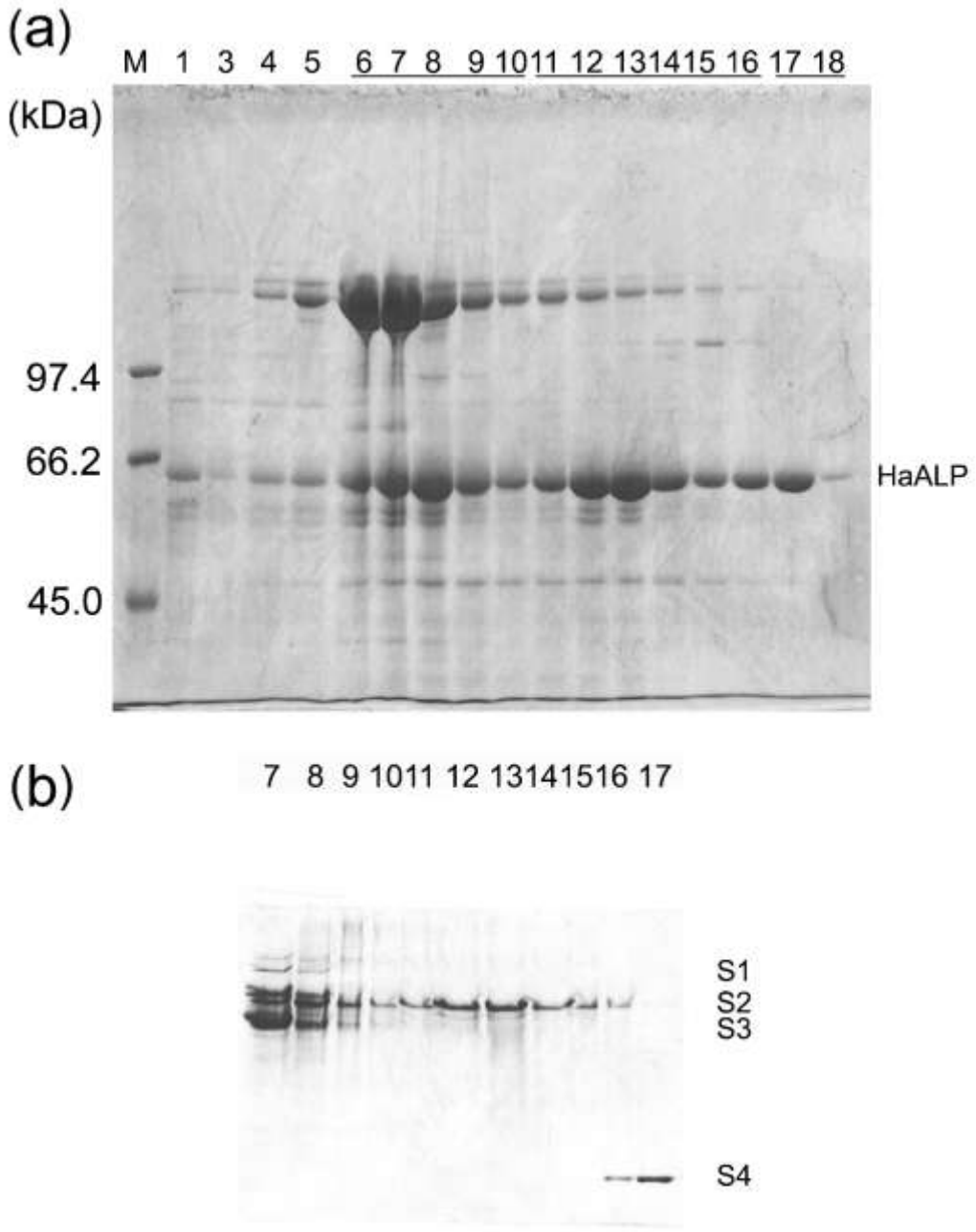

Fig. IV-2 SDS-PAGE (a) and native-PAGE (b) of HaALP purified by HiTrap Q HP.

HaALP was expressed by *B. choshinensis* in culture medium in the absence of NaCl. (a) HaALP shown next to the far-right lane indicates the mobility in 8% SDS-PAGE. (b) S1, S2, S3, and S4 shown next to the far-right lane indicates the mobility in 10% native-PAGE.

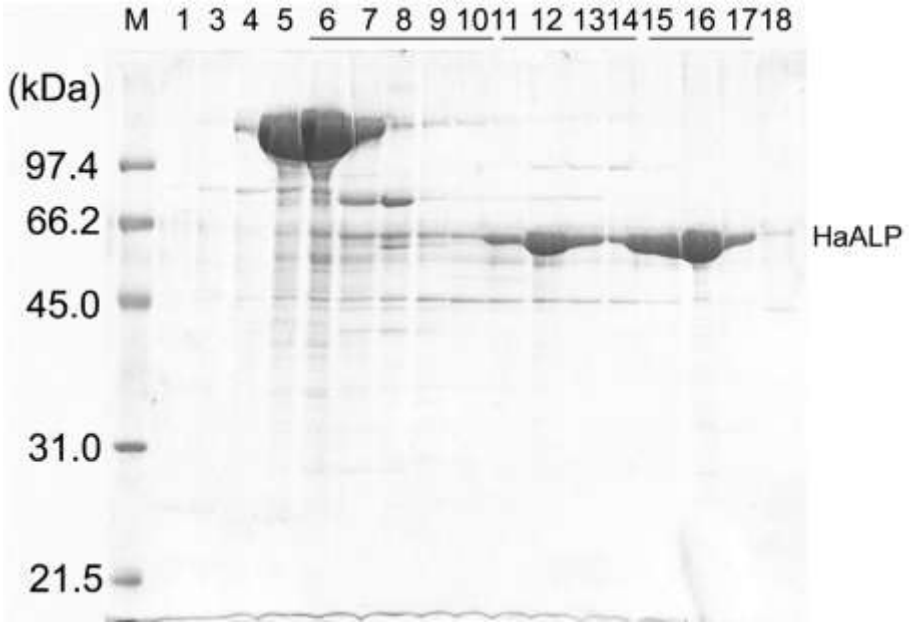

Fig. IV-3 SDS-PAGE of HaALP purified by HiTrap Q HP. HaALP was expressed by B. choshinensis in culture medium containing 0.2 M NaCl. HaALP shown next to the far-right lane indicates the mobility in 10% SDS-PAGE.

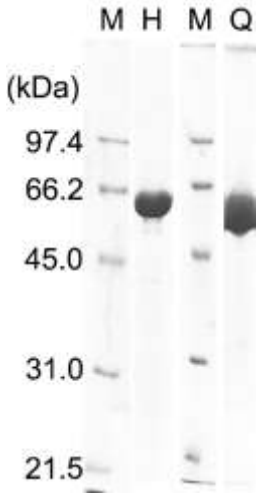

Fig. IV-4 SDS-PAGE of purified HaALP secreted in B. choshinensis using 10 % acrylamide gels. Lanes: M, molecular weights; H, purified HaALP after HisTrap HP chromatography; and Q, purified HaALP after HiTrap Q HP chromatography.

Table IV-3. Summary of purification by two-step chromatography

Purification steps	Total protein (mg)	Total activity (U)	Specific activity (U mg^{-1})	Fold	Yield (%)
Culture supernatant	1660	56500	34.0	1.00	100
HisTrap™ HP	5.50	34900	6340	186	62.0
Thrombin digestion					
HiTrap™ Q HP	3.20	21500	6680	196	38.0

For HaALP purification, 100 mL of culture supernatant was used

IV-3.2 Refolding of HaALP under Different Salt Conditions

We previously reported that the S3 folding intermediate, which was estimated to be about 45 kDa from gel filtration, of HaALP expressed by *E. coli* was converted to active dimer HaALP (S4). The molecular weight of this active dimer was estimated to be about 86 kDa from gel filtration, and it was produced only via the addition of Na^+ ions, suggesting the importance of Na^+ ions for HaALP structural maintenance [23]. To study the effects of HaALP refolding and Na^+ ions in detail, HaALP was completely denatured via urea, and activity was measured as an indicator of refolding under different conditions. High salt conditions are known to facilitate the refolding and activation of denatured halophilic enzymes [73, 74]. As shown in Fig. IV-5A, HaALP was refolded only in a buffer containing 3 M NaCl. To evaluate the folded structure, native PAGE was performed. The area (protein amount) in the band (S4) in Fig. IV-5B was also measured using ImageJ software. The amount of active HaALP (S4) increased as the specific activity increased daily in 3 M NaCl (Fig. IV-5A, B). The irreversible denaturation structure (S2) was found in all lanes, including before refolding (day 0). The specific activity was 1053 U/mg, which was 15.8% activity compared with the level of purified HaALP, on day 5 in 3 M NaCl (Fig. IV-5A). Other high-concentration salts [KCl, KBr, LiCl, $(NH_4)_2SO_4$, and $MgCl_2$] could not refold HaALP. However, 1.5 M Na_2SO_4 resulted in minimal HaALP refolding, and concentrations greater

than 1.5 M Na_2SO_4, involving more highly hydrophobic environments, could not be used because the solubility of Na_2SO_4 is low in water.

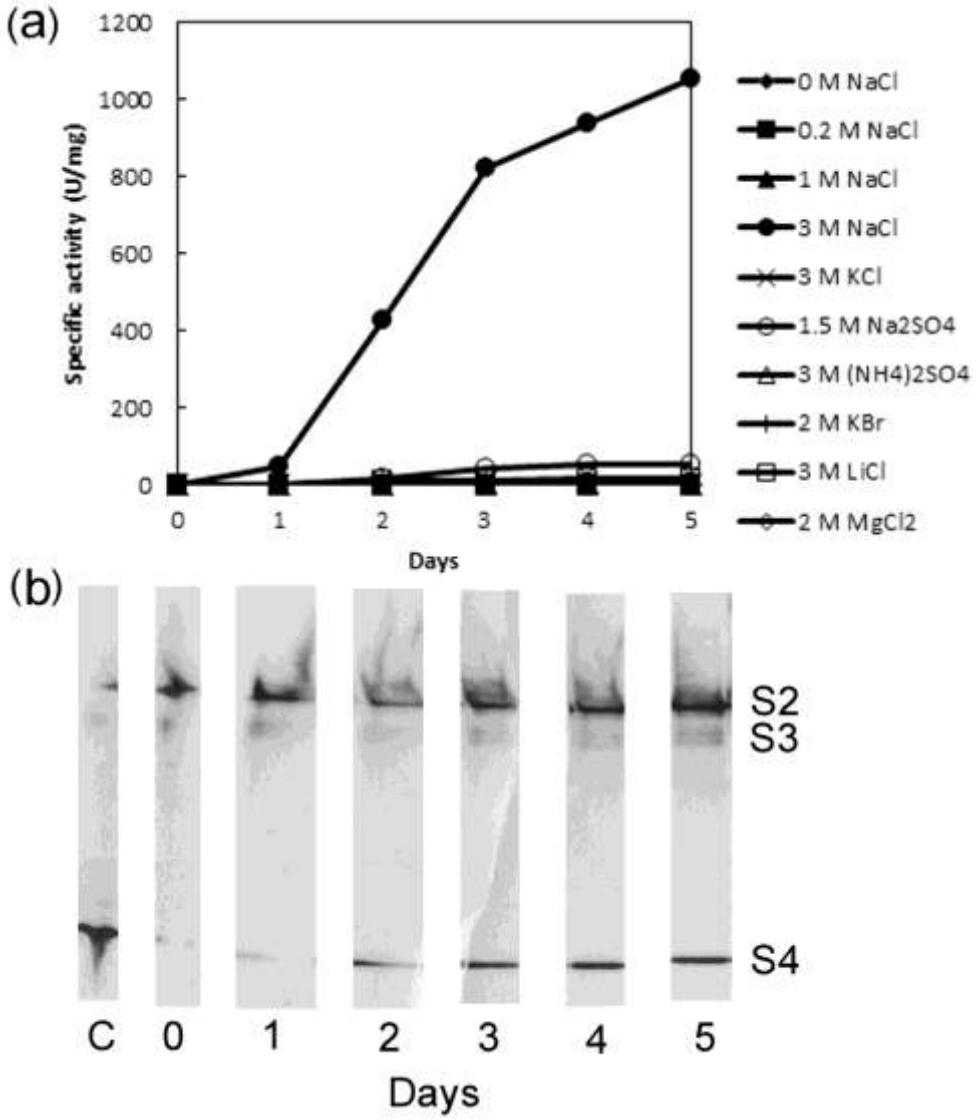

Fig. IV-5 Effects of different salts on HaALP refolding. (a) Samples denatured in 6 M urea were diluted into refolding buffer (pH 8.0) containing different salts and assayed for enzymatic activity as a function of time for five days. The HaALP concentration in the refolding buffer was 40 μg/ml. Results shown are average data of triplicate experiments, and deviation is less than 10%. (b) Sample aliquots (filled circle) in 3 M NaCl were collected every day and then subjected to native-PAGE.

IV-3.3 Refolding of HaALP by TMAO

Halophilic proteins contain a large excess of acidic amino acids on the surface, resulting in the requirement of salts such as NaCl to maintain stability to prevent repulsion among negative charges [62–64, 75]. Salts can also enhance hydrophobic interactions, leading to protein folding [76, 77]. To distinguish the effects of salts on halophilic proteins, a non-ionic osmolyte, trimethylamine N-oxide (TMAO), was used to assess HaALP folding. TMAO should have no charge-shielding effects and not undergo ionic binding. TMAO has been shown to accumulate in cells to raise the osmotic pressure and counteract the harmful effects of urea in kidney cells [69, 78, 79]. It is a strong protein stabilizer, increases the melting temperature, and induces protein folding.

As shown in Fig. IV-6A, 3 M TMAO could not refold HaALP. However, in the presence of low concentrations of NaCl (i.e., 0.2 M NaCl), which cannot cause the refolding of HaALP independently, TMAO could enhance HaALP folding. The addition of 3 M NaCl to a buffer containing 3 M TMAO resulted in a specific activity of 3851 U/mg on day 2 (Fig. IV-6A), which was a 58% activity compared with the activity of purified HaALP. This indicated the facilitation of refolding compared with refolding in the presence of only 3 M NaCl. To evaluate the folded structure, native PAGE was performed (data not shown). The amount of the S4 structure also increased as the specific activity increased, and similar to our NaCl refolding experiment, the irreversible denaturation structure (S2) was found in all lanes, including the one for day 0. Hence, the specific activity of refolded HaALP is considered to be lower than that of purified HaALP because of sub-divisional aggregation. Conversely, the specific activity decreased from day 3 in the refolding buffer containing 3 M TMAO and 3 M

NaCl, indicating that strong hydrophobic interactions caused by 3 M TMAO and 3 M NaCl enhanced destabilization during refolding.

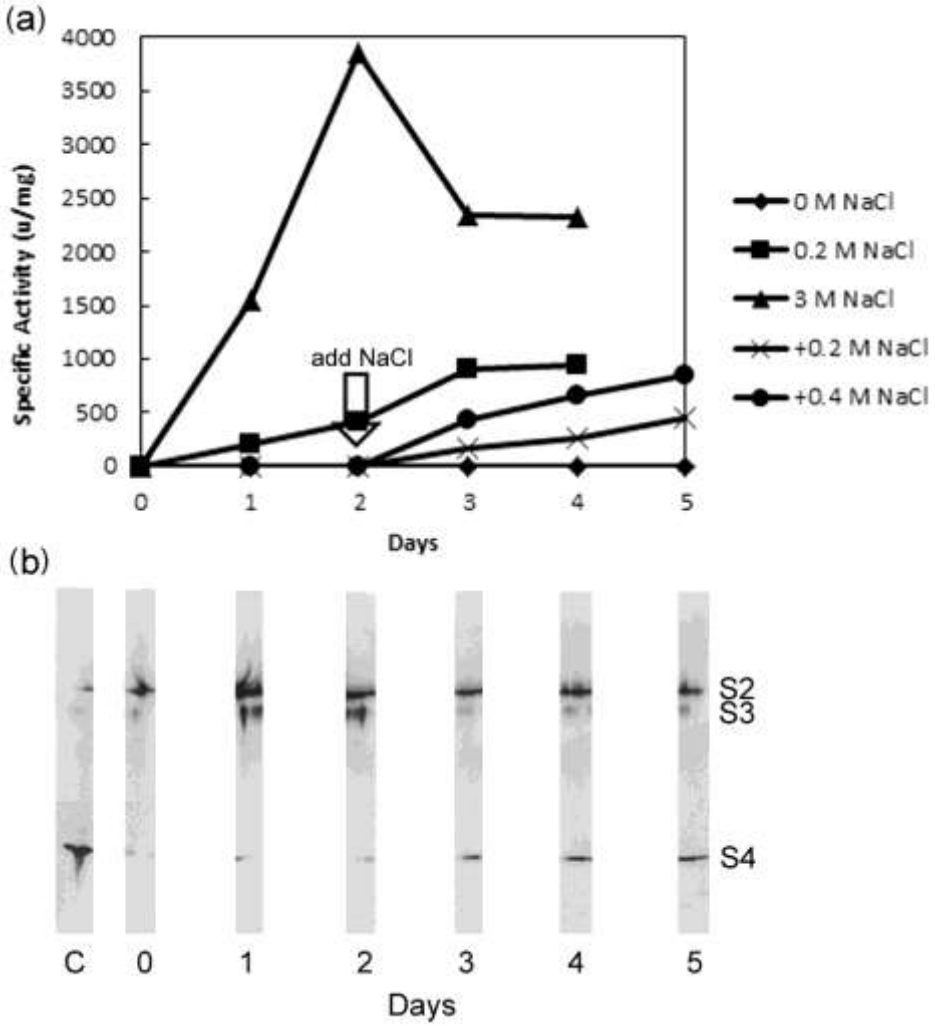

Fig. IV-6 Synergistic effects of TMAO and NaCl on HaALP refolding. (a) Samples denatured in 6 M urea were diluted into refolding buffer (pH 8.0) containing 3 M TMAO and NaCl (0–3 M) and assayed for enzymatic activity as a function of time for 4 or 5 days. The HaALP concentration in the refolding buffer was 40 μg/ml. After 2 days, 0.2 or 0.4 M NaCl was added to the refolding buffer of two samples, labelled as x and filled circle (shown by arrow). Results shown are the average data of triplicate experiments, and deviation is less than 10%. (b) Sample aliquots (filled circle) in 3 M TMAO, with 0.4 M NaCl added on day 2, was collected every day and then subjected to native-PAGE

Next, HaALP was refolded in a buffer containing 3 M TMAO in the absence of NaCl for 2 days, and then, 0.2–0.4 M NaCl was added to the refolding buffer. As a result, the addition of 0.2 M NaCl, which cannot enhance HaALP refolding independently, was sufficient to fold HaALP. The addition of 0.4 M NaCl further enhanced folding efficiency (Fig. IV-6A). To evaluate the folded structure, native PAGE was performed. The areas (protein amount) in the band of S3 and S4 in Fig. IV-6B were also measured using ImageJ software. As shown in Fig. IV-6B, the S3 structure (the folding intermediate) was present. There was almost no S4 structure (active dimer structure) on days 1 and 2 (Fig. IV-6B). The S4 structure was found from day 3 onward (after the addition of NaCl) and its level increased with a drastic decrease in the level of the S3 structure (Fig. IV-6A, B). These results suggest that 3 M TMAO can enhance the monomer S3 forms but cannot independently lead to the active dimer S4 form. However, in the presence of low concentrations of NaCl, active dimer forms (S4) resulted from S3 intermediates. The addition of salts, 0.2 M KCl, 0.1 M Na_2SO_4, 0.2 M $(NH_4)_2SO_4$, and 0.2 M LiCl, to a buffer containing 3 M TMAO after 2 days resulted in specific activities of 14%, 82%, 2%, and 2%, respectively, on day 7 compared with the addition of 0.2 M NaCl (data not shown), showing that Na_2SO_4 can activate the active dimer S4 forms. Further, 0.2 M KCl caused partial activation in the presence of 3 M TMAO, although this was as low as 14%, indicating that Na^+ ions are stronger activators than K^+ ions. These experimental results clearly show that Na^+ ions are required for the activation of HaALP dimer forms.

IV-4. Discussion

The stability of halophilic proteins requires not only a high salt concentration but also specific ion binding. HaALP also requires NaCl at a concentration of more than 0.3 M for its stability [24]. In this study, we highlighted the role of Na^+ ions in HaALP stability. Our study revealed that Na^+ ions were required for HaALP activation.

We previously attempted to express halophilic HaALP in non-halophilic *E. coli*. However, *E. coli* lacked the necessary high salt concentration to help with protein folding, and chaperones may help in the refolding of structures such as S1, S2, S3, and S4. [23]. HaALP is a periplasmic enzyme. Hence, we used a *Brevibacillus* expression system, which can efficiently secrete recombinant proteins. Our results showed that halophilic HaALP was successfully secreted as active HaALP in a non-halophile host. However, inactive HaALP was also found because it requires more than 0.3 M NaCl for stability [24]. Secreted active dimer HaALP (S4) may lead to inactive monomer HaALP structures (S1, S2, and S3), or secreted monomer HaALP precursors (folding intermediates, S3) may lead to non-reversible denaturation structures (S1 and S2) during cultivation (Fig. IV-2). Therefore, 0.2 M NaCl was added to the culture medium to prevent denaturation and/or to activate the active dimer forms. The associated results showed an increase in the abundance of active HaALP. This indicated that active HaALP (S4) was stabilized, or precursor HaALP (S3) was stabilized and activated to S4 via the addition of 0.2 M NaCl to the culture medium (Fig. IV-3). Thus, this protocol of using the *Brevibacillus* expression system succeeded in producing halophilic active HaALP.

Next, we successfully obtained His-tagged HaALP using *B. choshinensis*, in contrast to the case with *E. coli*. Hence, HaALP was highly purified by two-step chromatography and was used in the folding experiment. Purified HaALP was denatured completely using urea

and was then refolded under conditions with different salt concentrations. As shown in Fig. IV-5A, refolding from complete denaturation required a high NaCl concentration, such as 3 M, whereas low concentrations, such as 0.2 M NaCl, could not achieve the refolding of HaALP. This indicates that HaALP folding could be enhanced via hydrophobic interactions. However, other salts [KCl, KBr, LiCl, $(NH_4)_2SO_4$, and $MgCl_2$] could not refold HaALP, even at high concentrations, although 1.5 M Na_2SO_4 resulted in minimal HaALP refolding (Fig. IV-5A). This indicated that forming active HaALP also requires Na^+ ions. The refolding efficiency in 3 M NaCl was 15.8% based on purified HaALP activity, indicating that complete refolding may require not only 3 M NaCl but also other factors such as chaperones to prevent aggregation.

Conversely, a strong protein stabilizer, TMAO, which should have no charge-shielding effects or ionic binding, could not refold HaALP, even at high concentrations (Fig. IV-6A), whereas folding intermediates (S3),which was previously estimated to be about 45 kDa (the active dimer structure is 108 kDa) from gel filtration and was predicted with a monomer [23], were found in 3 M TMAO via native PAGE (Fig. IV-6A, B on days 1 and 2). This indicates that forming the S3 structure requires no salts and could be enhanced via thermodynamic interactions. The addition of 3 M NaCl to a refolding buffer containing 3 M TMAO showed 58% refolding efficiency based on the purified HaALP activity, indicating the facilitation of refolding compared with refolding in only 3 M NaCl. However, this condition did not lead to complete refolding. These results suggest that the complete refolding requires 3 M TMAO, 3 M NaCl, and other factors such as chaperones. When a small amount of NaCl was added to the refolding buffer containing 3 M TMAO after 2 days, refolding started (Fig. IV-6A), and active HaALP (S4),which was previously estimated to be about 86 kDa (the active dimer structure is 108 kDa) from gel filtration [23], was found via native PAGE from day 3 (Fig. IV-6A, B), indicating that just the addition of low-NaCl

solution, which cannot refold denatured HaALP independently, can form the active dimer S4 from the monomer S3. Although the addition of 0.2 M NaCl could activate S4 from S3 (Fig. IV-6A), the addition of other salts [0.2 M KCl, 0.2 M $(NH_4)_2SO_4$, and 0.2 M LiCl] could not really activate S4, except for the addition of Na_2SO_4 (82% activity compared with that of 0.2 M NaCl). This suggests that Na^+ ions are important for HaALP activation. In addition, HaALP activation increased in the refolding buffer containing 0.4 M NaCl, indicating a weak binding affinity for Na^+.

As mentioned above, when HaALP was secreted into the culture medium in the absence of NaCl by *B. choshinensis*, a HaALP precursor (S3) was found. However, in the presence of 0.2 M NaCl, S3 decreased, and active HaALP (S4) increased. This suggests that the HaALP precursor could be activated or the active HaALP could be stabilized by 0.2 M NaCl. This was consistent with our folding-experiment findings, showing the importance of Na^+ ions for HaALP stability.

With reference to the HaALP structure (PDB ID: 3WBH) [61], we predicted two possible Na^+ binding sites near the interface of the dimer (Fig. IV-7) based on the ideal distance (2.34–2.81 Å) between O and Na^+ [80]. We could not find Na^+ binding sites other than at the dimer interface. Fig. IV-7 showed that the coordination number of these candidates is low and the binding distance is somewhat long, indicating a weak binding affinity for Na^+. This is consistent with the findings from our folding experiment. These possible Na^+ binding sites may become a key for solving the HaALP folding and stabilization mechanism.

In conclusion, we successfully expressed halophilic HaALP using the non-halophile host *B. choshinensis* and revealed the role of Na^+ ions in HaALP stability and structure. Forming the folding intermediate required no salts. The monomer precursor HaALP was

activated to the active dimer form by Na^+ ions. Determination of the Na^+ ion binding site and binding mode remains the key for clarifying the HaALP folding and stabilization mechanism.

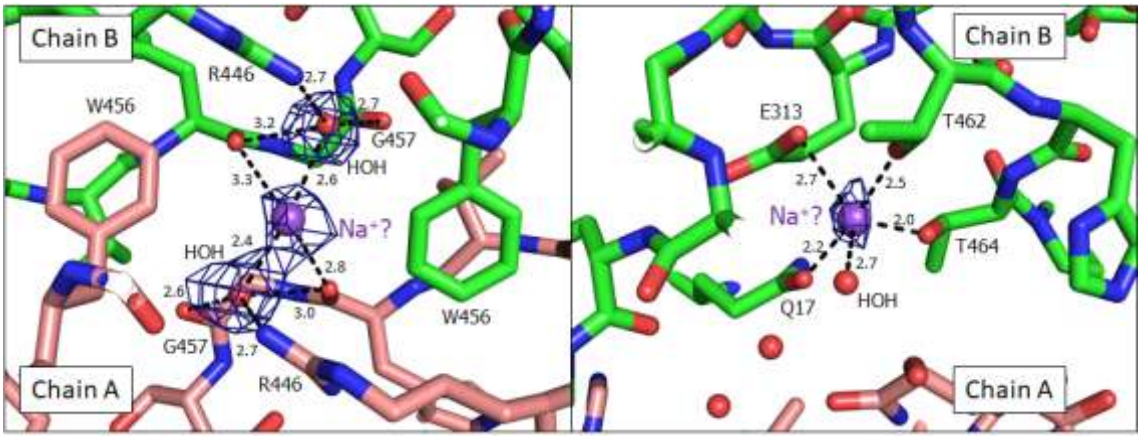

Fig. IV-7 Structure model of the area surrounding atoms, which might be involved in Na^+ ion binding to HaALP. To predict the Na+ ion binding sites in the HaALP molecule, the crystal structure of HaALP (PDB ID: 3WBH) was inspected as follows. Water molecules in the coordinate of 3WBH were rearranged based on the 2Fo – Fc electron density map with 1σ contour level. Then the ionic bond distances and the geometries of acceptor atoms (O atoms) were evaluated to identify the Na+ candidates from the rearranged water molecules [1, 2]. The distribution of the ionic bond distance between the acceptor and the Na+ ion (2.34–2.81 Å for Na – O) calculated from ionic radius [19] was included as criteria to identify the Na+ candidates. Blue meshes show the Fo – Fc OMIT map (1.5σ level).

V.

Summary

Enzymes from extremophiles have a great potential as industrially important enzymes. These enzymes have stability under extreme conditions that are attractive for use in industrial application. In this study, a thermophilic L-arabinose isomerase (L-AI) and a halophilic alkaline phosphatase from *Geobacillus stearothermophilus* and *Halomonas* sp. 593, respectively, were used and their properties were improved to cope with industrial demands. L-AI is an enzyme that converts D-galactose to D-tagatose, a prospective functional sweetener. L-AI from thermophilic bacterium, *G. stearothermophilus*, (GSAI) is expected to be a thermostable L-AI, which is a desirable trait for D-tagatose production. Nevertheless, the production of D-tagatose by L-AI faces several drawbacks that need to be improved for industrial application, e.g. improvement of substrate specificity of L-AI for D-galactose and increase the activity under acidic condition. On the other hand, halophilic enzymes easily degrade when used for industrial applications compared with enzymes from other extremophiles because of their instability in low-salt environments. Therefore, in this study, we aim to modify GSAI particularly in term of its substrate specificity for D-galactose and its activity under acidic condition and also clarify the stabilization mechanism of halophilic alkaline phosphatase.

We successfully obtained a mutant of GSAI, H18T, which exhibited increased activity for D-galactose compared with the wild-type (WT) enzyme. Substrate specifity of H18T for D-galactose was 45.4% higher than that of WT. Our investigation also showed that mutation at residue 18 from histidine to threonine resulted in 2.7-fold and 1.8-fold higher substrate binding and catalytic efficiency, respectively, for D-galactose. We performed comparison-based modeling to investigate the cause of higher affinity for D-galactose after mutation at residue 18. Investigation using normal mode analysis (NMA) software showed that replacing histidine with threonine at residue 18 increased the structural flexibility around the binding pocket; thus, resulted in better accessibility of D-galactose to bind at the binding

pocket. The addition of borate during L-arabinose isomerase catalysis further enhanced the specific activity and catalytic efficiency of H18T for D-galactose by up to 2.7-fold and 4.3-fold, respectively. H18T also showed thermostability and no destabilization was detected.

Although, H18T exhibited an excellent thermostability, its activity under acidic condition was not optimal. To enhance the activity of H18T under acidic condition, EP-PCR was performed around the binding pocket of H18T. We successfully obtained potential variant of H18T, H18TY234C, which showed improved activity at pH 6.0. H18TY234C demonstrated a 3-fold higher specific activity than WT at pH 6.0, but only 2-fold higher specific activity at pH 6.5-8.0, indicating a broadened optimal pH range of activity from 6.5-8.0 to 6.0-8.0. Analysis on the kinetic parameter of H18TY234C showed that the improvement at pH 6.0 may cause by the K_m as the k_{cat} decreased compared with the k_{cat} at pH 7.5, a similar trend with the parent H18T, but the K_m also decreased slightly, an opposite pattern with the parent H18T. Meanwhile, the higher activity at pH 6.5-8.0 was likely related with k_{cat} because H18TY234C displayed similar the K_m with the parent H18T but higher the k_{cat} than that of the parent H18T. Our investigation also showed that there is no formation of disulfide bonds after mutation from Tyrosine to Cysteine at residue 234. In addition, analysis using CD spectra also suggested that mutation did not affect the secondary structure of GSAI. On the other hand, computational investigation indicated higher flexibility at residue 229-236 and also higher the predicted pK_a value of residue 261, which is positioned at the opposite side of residue 234. Thus, the increase activity at pH 6.0 was not caused by the formation of disulfide bonds nor it was related with the secondary structure of the protein. Instead, it is likely caused by the change in the binding pocket area involving residue 234. Nevertheless, residue 234 was located far away from the active site. Hence, we speculate that the increase on the flexibility and the pK_a shift may indirectly affect the binding pocket via protein motion and/or allosteric effect.

Meanwhile, we also attempt to clarify the stabilization mechanism of *Halomonas* sp. 593 alkaline phosphatase (HaALP) by investigating the effects of salts on HaALP. The active form of HaALP was successfully obtained after HaALP was overexpressed in *Brevibacillus chosinensis* expression system and its purified fraction was used for evaluating the refolding of HaALP. HaALP was denatured in 6 M urea, refolded using various salts and the non-ionic osmolyte trimethylamine N-oxide (TMAO), and assessed by native polyacrylamide gel electrophoresis. HaALP refolded in 3 M NaCl or 3 M TMAO containing Na^+ ions. Hydrophobic interactions due to a high salt concentration or TMAO enhanced the formation of the folding intermediate (the monomer precursor), and only Na^+ ions activated the dimer form.

In conclusion, we successfully obtained a double-site variant of GSAI, H18TY234C, that displayed higher affinity for D-galactose and also possessed a broadened optimal pH toward acidic condition. Therefore, the double-site variant enzyme may be valuable in industrial D-tagatose production. In addition, we successfully showed the importance of Na^+ ions for HaALP stability. This insight into the stabilization mechanism of HaALP may lead to the development of industrial applications of halophilic enzymes under low-salt conditions.

V.

References

[1] L. Kumar, G. Awasthi, B. Singh, Extremophiles: a novel source of industrially important enzymes, Biotechnol. 10 (2) (2011) 121–135.

[2] J.A. Littlechild, Enzymes from extreme environments and their industrial application, Front. Bioeng. Biotechnol. 3 (2015) 161.

[3] P.S.J Chetham, and A.N. Wootton, Bioconversion of D-galactose into D-tagatose, Enzym. Microb. Technol. 15 (1993) 105–108.

[4] G.V. Levin, Tagatose, the new GRAS sweetener and health product, J. Med. Food 5 (2002) 23–26. https://doi.org/10.1089/109662002753723197.

[5] D.K. Oh, Tagatose: properties, applications, and biotechnological processes, Appl. Microbiol. Biotechnol. 81 (2007) 283–290.

[6] P. Kim, Current studies on biological tagatose production using L-arabinose isomerase: A review and future perspective, Appl. Microbiol. Biotechnol. 65 (2004) 243–249.

[7] Y.H. Hong, D.W. Lee, S.J. Lee, E.A. Choe, S.B. Kim, Y.H. Lee, C.I. Cheigh, Y.R. Pyun, Production of D-tagatose at high temperatures using immobilized *Eschericia coli* cells expressing L-arabinose isomerase from *Thermotoga neapolitana*, Biotechnol. Lett. 29 (4) (2007) 569–574.

[8] M. Rhimi, S. Bejar, Cloning, purification and biochemical characterization of metallic ions independent and thermoactive L-arabinose isomerase from *Bacillus stearothermophilus* US100 strain, Biochim. Biophis. Acta. 1760 (2006) 191–199.

[9] C. Fan, K. Liu, T. Zhang, L. Zhou, D. Xue, B. Jiang, W. Mu, Biochemical characterization of a thermostable L-arabinose isomerase from a thermoacidophilic bacterium, *Alicyclobacillus hesperidum* URH17-3-68, J. Mol. Catal. B Enzym. 102 (2014) 120–126.

[10] H.P. Modarres, M.R. Mofrad, A. Sanati-Nezhad, Protein Thermostability Engineering, RSC Adv. 6 (2016) 115252–115270.

[11] B.C. Kim, Y.H. Lee, H.S. Lee, D.W. Lee, E.A. Choe, Y.R. Pyun, Cloning, expression, and characterization of L-arabinose isomerase from *Thermotoga neapolitana*: bioconversion of D-galactose to D-tagatose using the enzyme, FEMS Microbiol. Lett. 212 (2002) 121–126.

[12] D.W. Lee, H.J. Jang, E.A. Choe, B.C. Kim, S.J. Lee, S.B. Kim, Y.H. Hong, Y.R. Pyun, Characterization of a thermostable L-arabinose (D-galactose) isomerase from hyperthermophilic eubacterium *Thermotoga maritima*, Appl. Environ. Microbiol. 70 (2004) 1397–1404. https://doi.org/10.1128/AEM.70.3.1397-1404.2004.

[13] Y. Li, Y. Zhu, A. Liu, and Y. Sun, Identification and characterization of a novel L-arabinose isomerase from *Anoxybacillus flavithermus* useful in D-tagatose production, Extremophiles 15 (2011) 441–450.

[14] F. Jorgensen, O.C. Hansen, and P. Stougaard, Enzymatic conversion of D-galactose to D-tagatose: heterologous expression and characterization of a thermostable L-arabinose isomerase from *Thermoanaerobacter mathranii*, Appl. Microbiol. Biotechnol. 64 (2004) 816–822.

[15] H.J. Kim, and D.K. Oh, Purification and characterization of an L-arabinose isomerase from an isolated strain of *Geobacillus thermodenitrificans* producing D-tagatose, J. Biotechnol. 120 (2005) 162–173.

[16] Z. Xu, S. Li, X. Feng, J. Liang, H. Xu, L-Arabinose isomerase and its use for biotechnological production of rare sugars, Appl. Microbiol. Biotechnol. 98 (2014) 8869–8878.

[17] S.J. Lee, D.W. Lee, E.A. Choe, Y.H. Hong, S.B. Kim, B.C. Kim, Y.R. Pyun, Characterization of a thermoacidophilic L-arabinose isomerase from *Alicyclobacillus acidocaldarius*: Role of Lys-269 in pH optimum, Appl. Environ. Microbiol. 71 (2005) 7888–7896.

[18] W. Xu, W. Zhang, T. Zhang, B. Jiang, W. Mu, L-Arabinose isomerases: Characteristics, modification, and application, Trends Food Sci. Tech. 78 (2018) 25–33.

[19] M. Kamekura , T. Hamakawa , H. Onishi, Application of halophilic nuclease H of *Micrococcus* varians subsp. *Halophilus* to commercial production of flavoring agent 5-GMP, Appl. Environ. Microbiol. 44 (1982) 994–995.

[20] A. Oren, Industrial and environmental applications of halophilic Microorganisms, Environ. Technol. 31(2010) 825–834.

[21] C.D. Litchfield, Potential for industrial products from the halophilic archaea, J. Ind. Microbiol. Biotechnol. 38 (2011) 1635–1647.

[22] T. Arakawa, H. Tokunaga, M. Ishibashi, M. Tokunaga, Halophilic properties and their manipulation and application. In: Singh OV (ed) Extremophiles: sustainable resources and biotechnological Implications, Wiley, Hoboken, (2012) pp 95–121.

[23] M. Ishibashi , O. Kazuki, T. Arakawa, M. Tokunaga, Cloning, expression, purification and activation by Na ion of halophilic alkaline phosphatase from moderate halophile Halomonas sp. 593, Protein Expr. Purif. 76 (2011) 97–102.

[24] M. Ishibashi, S. Yamashita, M. Tokunaga, Characterization of halophilic alkaline phosphatase from Halomonas sp. 593, a moderately halophilic bacterium, Biosci. Biotechnol. Biochem. 69 (2005) 1213–1216.

[25] J.M. Choi, Y.J. Lee, T.P. Cao, S.M. Shin, M.K. Park, H.S. Lee, E. di Luccio, S.B. Kim, S.J. Lee, S.J. Lee, S.H. Lee, D.W. Lee, Structure of the thermophilic L-arabinose

isomerase *Geobacillus kausthophilus* reveals metal-mediated intersubunit interactions for activity and thermostability. Arch. Biochem. Biophys. 596 (2016) 51–62.

[26] D. Fitriani, B. Saksono, Cloning of araA gene encoding L-arabinose isomerase from marine *Geobacillus stearothermophilus* isolated from Tanjung Api, Poso, Indonesia, Hayati J. Biosci. 17 (2) (2010) 58-62. https://doi.org/10.4308/hjb.17.2.58.

[27] U.K. Laemmli, Cleavage of structural proteins during the assembly of the head of bacteriophage T4, Nature 227 (1970) 680–685.

[28] P.K. Smith, R.I. Krohn, G.T. Hermanson, A.K. Mallia, F.H. Gartner, M.D. Provenzano, E.K. Fujimoto, N.M. Goeke, B.J. Olson, D.C. Klenk, Measurement of protein using bicinchoninic acid, Anal. Biochem. 150 (1985) 76–85.

[29] Z. Dische, and E. Borenfreund, A new spectrophotometric method for the detection and determination of keto sugars and trioses, J. Biol. Chem. 192 (2) (1951) 583–587.

[30] P. Emsley, K. Cowtan, *Coot*: model-building tools for molecular graphics, Acta Cryst. D60 (2004) 2126–2132.

[31] S.C. Lovell, I.W. Davis, W.B. 3rd Arendall, P.I. de Bakker, J.M. Word, M.G. Prisant, J.S. Richardson, D.C. Richardson, Structure validation by Cα geometry: ϕ, ψ and Cβ deviation, Proteins 50 (3) (2003) 437–50.

[32] J. Yu, Y. Zhou, I. Tanaka, M. Yao, Roll: A new algorithm for the detection of protein pockets and cavities with a rolling probe sphere. Bioinformatics. 26 (2010) 46-52. (http://altair.sci.hokudai.ac.jp/g6/service/pocasa/).

[33] H. Wako, S. Endo, Normal mode analysis as a method to derive protein dynamics information from the Protein Data Bank, Biophys. Rev. 9 (6) (2017) 877–893.

[34] N. Tokuriki, F. Stricher, L. Serrano, D.S. Tawfik, How protein stability and new functions trade off, PLoS. Comp. Biol. 4 (2) (2008) 1–7.

[35] N. Salonen, K. Salonen, M. Leisola, A. Nyssola, D-tagatose production in the presence of borate by resting *Lactococcus lactis* cell harboring *Bifidobacterium longum* L-arabinose isomerase, Bioprocess Biosyst. Eng. 36 (2013) 489-497.

[36] B.C. Lim, H.J. Kim, D.K. Oh, High production of D-tagatose by the addition of boric acid, Biotechnol. Prog. 23 (2007) 824–828.

[37] W.Y. Zhang, M. Jeya, J.K. Lee, L-ribulose production by an *Escherichia coli* harboring L-arabinose isomerase from *Bacillus licheniformis*, Appl. Microbiol. Biotechnol. 87 (2010) 1993–1999.

[38] P. Prabhu, M. Jeya, J.K. Lee, In silico studies on the substrate specificity of an L-arabinose isomerase from *Bacillus licheniformis*, Bioorg. Med. Chem. Lett. 20 (2010) 4436–4439.

[39] B.J. Kim, S.H. Hong, K.C. Shin, Y.S. Jo, D.K. Oh, Characterization of a F280N variant of L-arabinose isomerase from *Geobacillus thermodenitrificans* identified as a D-galactose isomerase, Appl. Microbiol. Biotechnol. 98 (2014) 9271–9281.

[40] N.G.H. Leferink, S.V. Antonyuk, J.A. Houwman, N.S. Scrutton, R.R. Eady, S.S. Hasnain, Impact of residues remote from the catalytic Centre on enzyme catalysis of copper nitrite reductase, Nat. Commun. 5 (4395) (2014) 1–7.

[41] E.O. McCullum, B.A.R. Williams, J. Zhang, J.C. Chaput, Random Mutagenesis by Error-Prone PCR, Methods Mol. Biol. 634 (2010) 103–9.

[42] C. Fan, W. Xu, T. Zhang, L. Zhou, B. Jiang, W.M. Mu, Engineering of *Alicyclobacillus hesperidum* L-arabinose isomerase for improved catalytic activity and reduced pH optimum using random and site-directed mutagenesis, Appl. Biochem. Biotechnol. 177 (2015) 1480–1492.

[43] F.A. Laksmi, S. Arai, H. Tsurumaru, Y. Nakamura, B. Saksono, M. Tokunaga, M. Ishibashi, Improved substrate specificity for D-galactose of L-arabinose isomerase for industrial application, BBA-proteins proteom. 1866 (2018) 1084–1091.

[44] K.P. Tan, T.B. Nguyen, S. Patel, R. Varadarajan, M.S. Madhusudhan, Depth: a web server to compute depth, cavity sizes, detect potential small-molecule ligand-binding cavities and predict the pKa of ionizable residues in proteins, Nucleic Acids Res. 41 (Web Server issue) (2013) W314–21.

[45] M. Rhimi, N. Aghajari, M. Juy, H. Chouayekh, E. Maguin, R. Haser, S. Bejar, Rational design of *Bacillus stearothermophilus* US100 Larabinose isomerase: potential applications for D-tagatose production, Biochimie 91 (5) (2009) 650–653.

[46] C. Wiedemann, P. Bellstedt, M. Görlach, CAPITO--a web server-based analysis and plotting tool for circular dichroism data, Bioinformatics 29 (14) (2013) 1750–7.

[47] S. Hammes-Schiffer and S.J. Benkovic, Relating protein motion to catalysis, Annu. Rev. Biochem. 75 (2006) 519–541.

[48] A. Tousignant and J.N. Pelletier, Protein motions promote catalysis, Chem. Biol. 11 (2004) 1037–1042.

[49] J.E. Coleman, Structure and mechanism of alkaline phosphatase, Annu. Rev. Biophys. Biomol. Struct. 21 (1992) 441–483.

[50] Y. Akiyama, K. Ito, Folding and assembly of bacterial alkaline phosphatase in vivo and in vitro, J. Biol. Chem. 15 (1993) 8146–8150.

[51] B. Stec, K.M. Holtz, E.R. Kantrowitz, A revised mechanism for the alkaline phosphatase reaction involving three metal ions, J. Mol. Biol. 299 (2000) 1303–1311.

[52] R.R. Jr Boulanger, E.R. Kantrowitz, Characterization of a monomeric *Escherichia coli* alkaline phosphatase formed upon a single amino acid substitution, J. Biol. Chem. 278 (2003) 23497–23501.

[53] P.S. Fitt, P. Baddoo, Separation and purification of the alkaline phosphatase and a phosphodiesterase from *Halobacterium cutirubrum*, Biochem. J. 181 (1979) 347–353.

[54] S. Goldman, K. Hecht, H. Eisenberg, M. Mevarech, Extracellular Ca^{2+}-dependent inducible alkaline phosphatase from extremely halophilic archaebacterium Haloarcula marismortui, J. Bacteriol. 172 (1990) 7065–7070.

[55] M.L. Bonet, F.I. Llorca, E. Cadenas, Kinetic mechanism of *Halobacterium halobium* Mn^{2+}- activated alkaline phosphatase, Biochem. Mol. Biol. Int. 34 (1994) 1109–1120

[56] F.C. Marhuenda-Egea, S. Piera-Velazquez, C. Cadenas, E. Cadenas, Mechanism of adaptation of an atypical alkaline p-nitrophenyl phosphatase from the archaeon *Halobacterium salinarum* at low-water environments. Biotechnol. Bioeng. 78 (2002) 497–502.

[57] A. Wende, P. Johansson, R. Vollrath, M. Dyall-Smith, D. Oesterhelt, M. Grininger, Structural and biochemical characterization of a halophilic archaeal alkaline phosphatase, J. Mol. Biol. 400 (2010) 52–62.

[58] M. Hayashi, T. Unemoto, M. Hayashi, pH- and anion-dependent salt modifications of alkaline phosphatase from a slightly halophilic *Vibrio alginolyticus*, Biochim. Biophys. Acta. 315 (1973) 83–93.

[59] N.K. Roy, R.K. Ghosh, J. Das, Monomeric alkaline phosphatase of *Vibrio cholera*, J. Bacteriol. 150 (1982) 1033–1039.

[60] B. Asgeirsson, O.S. Andresso, Primary structure of cold adapted alkaline phosphatase from a *Vibrio* sp. as deduced from the nucleotide gene sequence, Biochim. Biophys. Acta 1549 (2001) 99–111.

[61] S. Arai, Y. Yonezawa, M. Ishibashi, F. Matsumoto, M. Adachi, T. Tamada, H. Tokunaga, M. Blaber, M. Tokunaga, R. Kuroki, Structural characteristics of alkaline phosphatase from the moderately halophilic bacterium *Halomonas* sp. 593, Acta. Crystallogr. D Biol. Crystallogr. 70 (2014) 811–820.

[62] D.J. Kushner, Life in high salt and solute concentrations: halophilic bacteria. In: Kushner DJ (ed) Microbial life in extreme environments, Academic Press, London, (1978) pp 317–368.

[63] D.J. Kushner, The Halobacteriaceae. In: Woese CR, Wolfe RS (eds) The bacteria, vol 8, Academic Press, Orlando, (1985) pp 171–214.

[64] J.K. Lanyi, Salt-dependent properties of proteins from extremely halophilic bacteria, Bacteriol. Rev. 38 (1974) 272–290.

[65] S. Paul, S.K. Bag, S. Das, E.T. Harvill, C. Dutta, Molecular signature of hypersaline adaptation: insights from genome and proteome composition of halophilic prokaryotes, Genome Biol. 9 (2008) R70.

[66] C. Ebel, P. Faou, B. Kernel, G. Zaccai, Relative role of anions and cations in the stabilization of halophilic malate dehydrogenase, Biochemistry 38 (1999) 9039–9047.

[67] C. Ebel, L. Costenaro, M. Pascu, P. Faou, B. Kernel, F. Proust-De Martin, G. Zaccai, Solvent interactions of halophilic malate dehydrogenase, Biochemistry 41 (2002) 13234–13244.

[68] D. Madern, C. Ebel, Influence of an anion-binding site in the stabilization of halophilic malate dehydrogenase from *Haloarcula marismortui*, Biochimie 89 (2007) 981–987.

[69] T. Arakawa, S.N. Timasheff, The stabilization of proteins by osmolytes, Biophys. J. 47 (1985) 411–414.

[70] M. Mizukami, H. Tokunaga, H. Onishi, Y. Ueno, H. Hanagata, N. Miyazaki, N. Kiyose, Y. Ito, M. Ishibashi, Y. Hagihara, T. Arakawa, A. Miyauchi, M. Tokunaga, Highly efficient production of VHH antibody fragments in *Brevibacillus choshinensis* expression system, Protein Expr. Purif. 105 (2015) 23–32.

[71] M. Mizukami, H. Hanagata, A. Miyauchi, *Brevibacillus* expression system: host-vector system for efficient production of secretory proteins, Curr. Pharm. Biotechnol. 11 (2010) 251–258.

[72] H. Hanagata, M. Mizukami, A. Miyauchi, Efficient expression of antibody fragments with the *Brevibacillus e*xpression system, Antibodies 3 (2014) 242–252.

[73] F. Cendrin, J. Chroboczek, G. Zaccai, H. Eisenberg, M. Mevarech, Cloning, sequencing, and expression in *Escherichia coli* of the gene coding for malate dehydrogenase of the extremely halophilic archaebacterium *Haloarcula marismortui*., Biochemistry 32 (1993) 4308–4313.

[74] C. Pire , J. Esclapez, J. Ferrer, M.J. Bonete, Heterologous overexpression of glucose dehydrogenase from the halophilic archaeon *Haloferax mediterranei*, an enzyme of the medium chain dehydrogenase/reductase family, FEMS Microbiol. Lett. 200 (2001) 221–227.

[75] D. Madern, C. Ebel, G. Zaccai, Halophilic adaptation of enzymes, Extremophiles 4 (2000) 91–98.

[76] W. Malende, C. Horvath, Salt effect on hydrophobic interactions in precipitation and chromatography of proteins: an interpretation of the lyotropic series, Arch. Biochem. Biophys. 183 (1977) 200–215.

[77] T. Arakawa, S.N. Timasheff, Preferential interactions of proteins with salts in concentrated solutions, Biochemistry 21 (1982) 6545–6552.

[78] Y. Liu, D.W. Bolen, The peptide backbone plays a dominant role in protein stabilization by naturally occurring osmolytes, Biochemistry 34 (1995) 12884–12891.

[79] A. Wang, D.W. Bolen, A naturally occurring protective system in urea-rich cells: mechanism of osmolyte protection of proteins against urea denaturation, Biochemistry 36 (1997) 9101–9108.

[80] W.M. Haynes, D.R. Lide, T.J. Bruno, CRC handbook of chemistry and physics, 94th edn. CRC Press, Boca Raton (2013).